

THE GEMINI DEEP DEEP SURVEY: II. METALS IN STAR-FORMING GALAXIES AT REDSHIFT $1.3 < z < 2^1$

S. SAVAGLIO^{2,3}, K. GLAZEBROOK², R. G. ABRAHAM⁴, D. CRAMPTON⁵, H.-W. CHEN^{6,7}, P. J. P. MCCARTHY⁸, I. JØRGENSEN⁹, K. C. ROTH⁹, I. M. HOOK¹⁰, R. O. MARZKE¹¹, R. G. MUROWINSKI⁵, R. G. CARLBERG⁴

ApJ in press

ABSTRACT

The goal of the Gemini Deep Deep Survey (GDDS) is to study an unbiased sample of $K < 20.6$ galaxies in the redshift range $0.8 < z < 2.0$. Here we determine the statistical properties of the heavy element enrichment in the interstellar medium (ISM) of a subsample of 13 galaxies with $1.34 < z < 1.97$ and UV absolute magnitude $M_{2000} < -19.65$. The sample contains 38% of the total number of identified galaxies in the first two fields of the survey with $z > 1.3$. The selected objects have colors typical of irregular and Sbc galaxies. Strong [O II] emission indicates high star formation activity in the H II regions ($\text{SFR} \sim 13 - 106 M_{\odot} \text{ yr}^{-1}$). The high S/N composite spectrum shows strong ISM Mg II and Fe II absorption, together with weak Mn II and Mg I lines. The Fe II column density, derived using the curve of growth analysis, is $\log N_{\text{FeII}} = 15.54^{+0.23}_{-0.13}$. This is considerably larger than typical values found in damped Ly α systems (DLAs) along QSO sight lines, where only 10 out of 87 ($\sim 11\%$) have $\log N_{\text{FeII}} \geq 15.2$. High Fe II column densities are observed in the $z = 2.72$ Lyman break galaxy cB58 ($\log N_{\text{FeII}} \simeq 15.25$) and in gamma-ray burst host galaxies ($\log N_{\text{FeII}} \sim 14.8 - 15.9$). Given our measured Fe II column density and assuming a moderate iron dust depletion ($\delta_{\text{Fe}} \sim 1$ dex), we derive an optical dust extinction $A_V \sim 0.6$. If the H I column density is $\log N_{\text{HI}} < 21.7$ (as in 98% of DLAs), then the mean metallicity is $Z/Z_{\odot} > 0.2$. The high completeness of the GDDS sample implies that these results are typical of star-forming galaxies in the $1 < z < 2$ redshift range, an epoch which has heretofore been particularly challenging for observational programs.

Subject headings: cosmology: observations – galaxies: abundances – galaxies: ISM

1. INTRODUCTION

The interstellar medium (ISM) is an important component in galaxies, not only in terms of mass, but also because it carries information on past generations of stars, and provides the main fuel for the new generations of stars. In the local Universe the cold ISM ($T \lesssim 1000$ K) is ~ 15 -40% of the total mass in stars (Fukugita et al. 1998; Zwaan et al. 2003), and at higher redshifts it is a major constituent of the Universe (~ 2 times higher than in the local Universe at $1.5 < z < 2.0$; Storrie-Lombardi & Wolfe 2000; Peroux et al. 2003). In the cold ISM, heavy elements – the footprint of the stellar activity – can most easily be investigated through the analysis of UV absorption lines.

Apart from very detailed analysis in Galactic ISM (Savage & Sembach 1996), in the local Universe exploring the UV

absorption lines become possible only for a few bright star-forming galaxies (Heckman et al. 2001; Aloisi et al. 2003) due to limited capabilities of UV satellites. At higher redshifts, bright QSO sources, whose sight lines cross intervening galaxies, allow the detection of absorption lines with UV satellites and (at $z > 2.5$) ground-based telescopes. QSO damped Lyman- α systems (QSO-DLAs) have probed the ISM in more than 100 galaxies at $0.0 < z < 4.5$ (Prochaska et al. 2003a). These data may be biased, however, to galaxies or regions of galaxies that are dust- and metal-poor since dusty, metal rich systems are likely to obscure or, at least, extinct the background QSO.

Indeed, we have indications that the ISM in other high redshift objects is chemically more evolved. For instance, gamma-ray burst (GRB) afterglows are associated with regions of intense star formation (Bloom, Kulkarni, & Djorgovski 2002; Djorgovski et al. 2003). They are – for a short time – much brighter than QSOs (~ 1000 times brighter in X-ray fluxes) and can be detected even if embedded in a very dense medium. The analysis of UV absorption lines in 4 GRB spectra (GRB-DLAs) shows high column density of metals in the ISM of the host galaxies (Savaglio, Fall, & Fiore 2003; Vreeswijk et al. 2003). In addition, large surveys of $z > 2.5$ Lyman-break galaxies (LBGs, Steidel et al. 2003) show predominantly high equivalent widths (EWs) of ISM metal absorption lines (Pettini et al. 2002; Shapley et al. 2003).

The direct study of cold ISM in galaxies requires reasonable S/N of the rest-frame UV continuum, and this is generally not sufficiently strong for our observational capabilities, even when redshifted to the optical at high z . Additionally, systematic problems arise from imperfect sky subtraction and CCD fringe removal. As a consequence, surveys have mainly targeted $z > 2.5$ galaxies where the Lyman-break technique starts to be effective, or strong emission line objects, observable in the optical up to $z \sim 1$. The $1 < z < 2.5$ range is often

¹ Based on observations obtained with the Gemini North Telescope

² Johns Hopkins University, 3400 North Charles Street, Baltimore, MD 21218; savaglio@pha.jhu.edu

³ On leave of absence from Osservatorio Astronomico di Roma, Italy

⁴ Department of Astronomy & Astrophysics, University of Toronto, 60 St. George Street, Toronto, ON, M5S 3H8, Canada

⁵ Herzberg Institute of Astrophysics, National Research Council, 5071 West Saanich Road, Victoria, British Columbia, V9E 2E7, Canada

⁶ Center for Space Research, Massachusetts Institute of Technology, Cambridge, MA 02139-4307

⁷ Hubble Fellow

⁸ Observatories of the Carnegie Institution of Washington, 813 Santa Barbara Street, Pasadena, CA 91101

⁹ Gemini Observatory, Hilo, HI 96720

¹⁰ Department of Astrophysics, Nuclear & Astrophysics Laboratory, Oxford University, Keble Road, Oxford OX1 3RH, UK

¹¹ Department of Physics and Astronomy, San Francisco State University, 1600 Holloway Avenue, San Francisco, CA 94132

¹² Herzberg Institute of Astrophysics, National Research Council, 5071 West Saanich Road, Victoria, British Columbia, V9E 2E7, Canada

¹³ Department of Astronomy & Astrophysics, University of Toronto, 60 St. George Street, Toronto, ON, M5S 3H8, Canada

referred to as the “redshift desert” for lack of discoveries. This interval is also very problematic for studies of galaxy evolution, since it apparently spans a major epoch of galaxy building: 50 – 75% of the stellar mass in galaxies was in place by $z \sim 1$, whereas at $2.5 < z < 3.5$ the Lyman break galaxies contain only ~ 3 –20% of the present day stellar mass (Dickinson et al. 2003; Fontana et al. 2003). Recently, the K20 survey (Cimatti et al. 2002a) with 82 spectroscopically confirmed $K < 20$ galaxies at $1 < z < 2$ have started to unveil some aspects of galaxy evolution in the redshift desert (Cimatti et al. 2002b; Pozzetti et al. 2003). However, the number of galaxies drops to 17 if the $1.3 < z < 2$ interval is considered.

To improve optical spectroscopy, a new observing mode known as Nod & Shuffle (N&S), has been recently developed (Glazebrook & Bland-Hawthorn 2001; Cuillandre et al. 1994). During N&S observations, the telescope is rapidly switched between object and sky positions (“nodding”), while the charge is “shuffled” between different parts of the CCD. Because both the sky and objects are observed through the same optical path, slits, and pixels, the effects of fringing are eliminated and the sky subtraction greatly improved. As a result, N&S allows very long integration times before systematic effects start to dominate, ~ 10 times longer than is practical with conventional spectroscopy.

We have begun a project to observe galaxies in the redshift desert (the Gemini Deep Deep Survey, GDDS, Abraham et al. in preparation) that uses the N&S technique on the multi-object spectrograph at the Gemini 8m telescope. The $\sim 10^5$ seconds exposures allow us to reach very faint magnitudes (limiting magnitude $I_{AB} = 24.8$ and $K = 20.6$, more than half a magnitude deeper than K20). Both raw and fully reduced data from the GDDS will be publicly available¹⁴. In this paper we present first results on the heavy element enrichment in the cold ISM of a subset of galaxies at $1.3 < z < 2.0$, based on observations of the first two fields. We estimate the column densities of Fe II, Mn II, and Mg II using the curve of growth analysis, and compare our results with what is already known of the ISM over a larger redshift scale.

The paper is structured as follows: in §2 we present the data set, the sample selection is described in §3, in §4 we report [O II] line flux measurements, in §5 we describe the method used to combine the individual spectra, in §6 we measure column densities of metals, in §7 we report results of other surveys, in §8 we discuss the general properties of the selected sample, and in §9 we summarize the main conclusions. Throughout the paper we adopt a $h \equiv H_0/100 = 0.7$, $\Omega_M = 0.3$, $\Omega_\Lambda = 0.7$ cosmology.

2. GDDS DATA

The spectra presented in this paper were obtained during three observing runs at the Gemini North telescope in the period 2002 August–October. The two fields SA22 ($\alpha_{2000} = 22^h17^m20^s$, $\delta_{2000} = +00^\circ21'30''$) and NDWS¹⁵ ($\alpha_{2000} = 02^h10^m00^s$, $\delta_{2000} = -04^\circ30'00''$) were selected from the Las Campanas Infrared (LCIR) Survey (McCarthy et al. 2001; Chen et al. 2002; Firth et al. 2002; Chen et al. 2003), and observed with the Gemini multi-object spectrograph (GMOS, $5.5' \times 5.5'$ field of view; Murowinski et al. in preparation; Hook et al. 2003). The “queue scheduled” mode at the Gem-

ini observatory ensured that data were taken only when the weather conditions were as requested. As a result, during our observations the seeing was $\lesssim 0.85''$ in I band for most of the time. The LCIR Survey photometry ($VIzHK$ filters for field SA22 and $BVRIZK$ filters for field NDWS) was used to pre-select $z > 0.8$ objects in the two fields with the photometric redshift technique. Two GMOS masks were used for field SA22 (exposure times 48600 and 90000 seconds) with 111 slits total, and one mask with 60 slits for field NDWS (exposure time 75600 seconds). The total number of objects observed was then 171. The observations were taken using $0.75'' \times 2.2''$ and $0.75'' \times 2''$ slit apertures. The comparison with similarly faint IR galaxies at $z > 1$ (Yan et al. 1998) suggests that the slit apertures allow to collect more than 50% of the galaxy flux. The 2D data reduction was performed using IRAF¹⁶ and Gemini/GMOS tools¹⁷. For the 1D spectrum extractions we used iGDDS, a package specifically written with the toolkit Cocoa under Mac OS X (details in Abraham et al. in preparation). Uncertainty in the wavelength calibration is of the order of 1.5 \AA . The wavelength calibrated spectra were corrected for the telluric absorption and flux calibrated. Most of the observations were carried out near transit and no corrections for differential atmospheric refraction (which is small at these wavelengths) were applied. To confirm that the N&S technique was working as expected, sky residuals were measured from some strong lines in a stack of 60 spectra. The residuals are of the order of 0.05–0.1%, as predicted by Glazebrook & Bland-Hawthorn (2001). The final spectral coverage in each spectrum is within the 5000–10000 \AA interval, depending on the position of the slit in the mask, and the dispersion is $\Delta\lambda \simeq 3.5 \text{ \AA}$ per pixel. The resolution element, determined by the slit width, is 4.5 pixels or $\text{FWHM} \simeq 16 \text{ \AA}$, equivalent to $960\text{--}460 \text{ km s}^{-1}$, from the blue to the red end of the spectral range. The resolution was also measured from unresolved sky emission lines to be $\text{FWHM} \simeq 17\text{--}18 \text{ \AA}$, slightly larger than the nominal resolution. This is not unexpected since the sky emission is extended over the whole slit aperture.

The spectra were extracted both using the linear and the optimal extraction method. In parallel the noise spectrum was created for each object using the object and sky extracted signal, and the read-out-noise of the instrument ($3\text{--}3.5 e^-$, depending on the CCD). Redshifts were found from simple eye inspection of line positions. Manual redshifting (possible thanks to the small number of spectra) was done because of the ability of the eye to reject extraneous data artifact features in the 2D spectrum. Among the 171 objects observed, 7 have been identified as stars, 4 as AGNs, 18 have tentative redshift, 18 have no redshift. The remaining 124 extragalactic objects have secure redshift.

3. SAMPLE SELECTION

To measure metal enrichment in galaxies in the $1 < z < 2.5$ range, we use absorption lines in the rest-frame interval 2200–2900 \AA . This is a particularly interesting region because it contains 7 Fe II transitions, with very different oscillator strengths, together with the strong Mg II doublet and the Mg I line. The Mg II doublet is normally very strong and

¹⁴ Data can be downloaded at the GDDS homepage <http://www.ociw.edu/lcirs/gdds.html>

¹⁵ NDWS: NOAO Deep Wide-Field Survey.

¹⁶ IRAF is distributed by the National Optical Astronomy Observatories, which are operated by the Association of Universities for Research in Astronomy, Inc., under cooperative agreement with the National Science Foundation.

¹⁷ For more information visit <http://www.gemini.edu/sciops/instruments/gmos/gmosIndex.html>

TABLE 1
SELECTED GALAXY SAMPLE

| GDDS ID | z_{ISM}^a | $z_{[\text{O II}]}^b$ | Δv^c (km s $^{-1}$) | K | $I-K$ | M_{2000}^d | $F_{[\text{O II}]}^e$ (10^{-17} erg s $^{-1}$ cm $^{-2}$) | $L_{[\text{O II}]}^f$ (10^{41} erg s $^{-1}$) | $\text{SFR}_{[\text{O II}]}^f$ (M_{\odot} yr $^{-1}$) | SFR_{2000}^g (M_{\odot} yr $^{-1}$) |
|---------|--------------------|-----------------------|---------------------------------|------------------|-----------------|--------------|--|--|--|---|
| 02-1417 | 1.5998 | 1.5990 | -92 | 19.85 ± 0.35 | 3.48 ± 0.35 | -19.70 | 3.19 ± 0.73 | 5.3 ± 1.2 | 13 | 20 |
| 02-1636 | 1.6357 | 1.6360 | +34 | 20.24 ± 0.42 | 3.07 ± 0.42 | -20.03 | 9.74 ± 0.84 | 17.1 ± 1.5 | 43 | 27 |
| 02-1790 | 1.5778 | 1.5767 | -128 | 20.64 ± 0.52 | 2.36 ± 0.52 | -20.70 | 26.00 ± 0.70 | 41.7 ± 1.1 | 106 | 49 |
| 02-2530 | 1.5278 | 1.5263 | -178 | 20.32 ± 0.44 | 2.67 ± 0.44 | -20.17 | 9.40 ± 0.69 | 13.9 ± 1.0 | 35 | 30 |
| 22-0964 | 1.5113 | 1.5124 | +131 | 19.61 ± 0.28 | 3.30 ± 0.28 | -19.81 | 4.61 ± 0.58 | 6.7 ± 0.8 | 17 | 22 |
| 22-1042 | 1.5228 | 1.5248 | +237 | 20.00 ± 0.34 | 3.17 ± 0.34 | -19.69 | 7.99 ± 0.51 | 11.8 ± 0.8 | 30 | 20 |
| 22-1055 | 1.3407 | 1.3410 | +38 | 19.47 ± 0.26 | 3.39 ± 0.26 | -19.70 | 4.21 ± 0.15 | 4.5 ± 0.2 | 12 | 20 |
| 22-1559 | 1.8954 | ... | ... | 20.74 ± 0.49 | 2.97 ± 0.49 | -20.56 | ... | ... | ... | 44 |
| 22-1909 | 1.4847 | 1.4876 | +350 | 20.81 ± 0.52 | 2.33 ± 0.52 | -20.43 | 8.62 ± 0.31 | 12.0 ± 0.4 | 30 | 39 |
| 22-2172 | 1.5613 | 1.5613 | 0 | 20.41 ± 0.41 | 2.69 ± 0.41 | -20.29 | 11.86 ± 0.56 | 18.6 ± 0.9 | 47 | 34 |
| 22-2264 | 1.6703 | 1.6742 | +438 | 20.60 ± 0.46 | 2.82 ± 0.47 | -20.35 | 17.03 ± 1.55 | 31.6 ± 2.9 | 80 | 36 |
| 22-2395 | 1.4847 | 1.4863 | +193 | 20.45 ± 0.42 | 2.46 ± 0.42 | -20.80 | 5.08 ± 0.34 | 7.0 ± 0.5 | 18 | 54 |
| 22-2400 | 1.9669 | ... | ... | 20.34 ± 0.41 | 3.14 ± 0.42 | -21.07 | ... | ... | ... | 69 |

^aRedshift of the ISM absorption lines.

^bRedshift of the [O II] emission line.

^cVelocity difference between $z_{[\text{O II}]}$ and z_{ISM} .

^dAB absolute magnitude in a synthetic box filter centered at $\lambda = 2000$ Å. The accuracy is ~ 0.2 magnitudes (see text).

^eThe [O II] fluxes have been measured from the spectra, and no aperture correction has been applied. Errors include only photon counting statistics.

^fSFRs are estimated assuming $\text{SFR}_{[\text{O II}]}(M_{\odot} \text{ yr}^{-1}) \simeq 2.54 \times L_{[\text{O II}]} \times 10^{-41} \text{ erg s}^{-1} \text{ cm}^{-2}$.

^gSFRs are estimated assuming $\text{SFR}_{2000}(M_{\odot} \text{ yr}^{-1}) \simeq 1.25 \times L_{2000} \times 10^{-28} \text{ erg s}^{-1} \text{ Hz}^{-1}$.

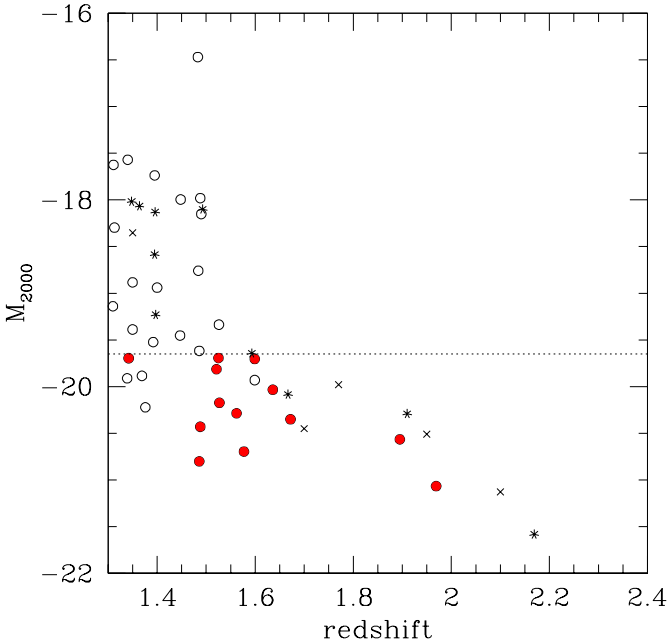


FIG. 1.— AB M_{2000} absolute magnitude of GDDS $1.3 < z < 2.4$ galaxies as a function of redshift. Fluxes are extracted from a 2 arcsec aperture. Open and filled dots are galaxies with secure spectroscopic redshift, respectively. Filled dots are the selected galaxies with $M_{2000} < -19.65$. Stars are objects with tentative redshift. Crosses have no spectroscopic redshift; in these cases we used the photometric redshift. The selected sample contains between 25 and 38% of the total number of galaxies identified in GDDS with $1.3 < z < 2.4$ (depending whether galaxies with tentative or photometric-redshift only are included in the count or not).

highly saturated but it is very useful in determining galaxy redshifts. The useful wavelength range for most GDDS spectra is limited to $\lambda = 5000 - 9800$ Å, or the rest-frame interval $\lambda = 2200 - 2900$ Å for galaxies at $1.3 < z < 2.4$. In the total sample of 124 objects with spectroscopic redshift in the two fields, 34 galaxies are in this z range. The number of objects with tentative or photometric-only redshifts in $1.3 < z < 2.4$ is 10 and 7, respectively.

For all $1.3 < z < 2.4$ objects, we estimated the AB absolute magnitude M_{2000} using a synthetic $1900 \text{ Å} < \lambda < 2100 \text{ Å}$ box filter derived from the observed V and I magnitudes (Fig. 1). To estimate M_{2000} for the galaxies in our sample we use the following empirical formula:

$$M_{2000} = V - 2f(1.72) + f(z) + 5.058 - 2.91z - 0.114(V - I)(z - 1.72) \quad (1)$$

where:

$$f(z) = 25 + 5 \log D_L(z) - 2.5 \log(1 + z) \quad (2)$$

and $D_L(z)$ is the luminosity distance in Mpc of galaxies at redshift z . Eqs. 1 and 2 were derived by us considering that to first order approximation the observed V band matches the rest M_{2000} band at $z = 1.72$. The extra terms represent the mean K -correction away from $z = 1.72$ and a small correction for its dependence on spectral energy distribution (SED) shape (parameterized by $V - I$ observed). The coefficients were derived by empirically fitting the observed colors to $1.3 < z < 2$ template spectra (Chen et al. 2002) ranging from E/S0 to Starburst SEDs; the formula was found to predict M_{2000} to < 0.2 mag accuracy over this entire redshift range for all SEDs. We emphasize that it is robust, model independent

(i.e. insensitive to SED shape) in this redshift range simply because the optical photometry samples the rest-frame UV.

Among the 34 galaxies with secure redshifts, we selected the brightest subsample with $M_{2000} < -19.65$ (Fig. 1). This subsample contains 17 galaxies, but three of them were not considered because the spectra are contaminated by second order lines, and a fourth because it has partial spectral coverage in the 2200–2900 Å range. The remaining 13 galaxies (Table 1) cover the range $1.34 < z < 1.97$ (mean and median redshift $z = 1.60$ and $z = 1.56$). In Table 1, we report redshifts independently derived from the ISM absorption lines and the [O II] emission line (when observed). The mean velocity difference between the [O II] emission and ISM absorption is $\Delta v = 93$ with 197 km s^{-1} dispersion. The observed $I-K$ colors (in the range $2.2 < I-K < 3.5$) are consistent with predictions derived from a suite of spectral synthesis models for Irr- or Scd-type galaxies. This sample represents 25% or 38% of the total number of GDDS galaxies in $1.3 < z < 2.4$, depending whether the objects with tentative spectroscopic or photometric-only redshifts are included in the counting or not.

4. THE [O II] EMISSION AND STAR FORMATION RATES

The [O II] $\lambda 3727$ emission line is detected in 11 of the 13 galaxies selected (Fig. 2). For the two highest redshift galaxies the [O II] wavelength is out of the observed spectral range. The presence of the [O II] nebular emission is another indication of star formation activity in these galaxies, as it is associated with H II regions. No other emission line is detected. The [O II] flux has been measured in the spectrum of each galaxy and reported in Table 1. As fluxes in the red end of the spectra are roughly consistent with the aperture corrected photometry, no aperture correction has been applied. Errors are derived using photon counting statistics only. Our spectral sensitivity is sufficiently good to detect very low fluxes, down to $\sim 2 \times 10^{-17} \text{ erg s}^{-1} \text{ cm}^{-2}$ ($\sim 3\sigma$) at $\lambda > 8600 \text{ Å}$. Observed fluxes, in the range $(3-26) \times 10^{-17} \text{ erg s}^{-1} \text{ cm}^{-2}$ and absolute luminosities $(5-42) \times 10^{41} \text{ erg s}^{-1}$ are reported in Table 1.

The star formation rate (SFR) in local H II regions is generally directly derived from optical Balmer lines (Gallagher, Hunter, & Bushouse 1989; Kennicutt 1992; Gallego et al. 1995). However, at high redshift, Balmer lines are redshifted to the IR, making the SFR measurement harder. If Balmer lines are not observed, the [O II] emission line can be used instead, since it is detectable in the optical up to $z \sim 1.6$. The problem is that [O II] gives a much less direct estimate of the SFRs, because it is more affected by dust than Balmer lines (for which dust correction can be easily determined), and because it depends on the electron temperature and metallicity of the H II region. In local galaxies, Jansen, Franx, & Fabricant (2001) found a correlation between [O II]/H α ratio and the galaxy absolute magnitude that allows to estimate the SFR if only the [O II] emission line and the M_B are known. Their Fig. 4a shows that for bright objects ($M_B < -20.5$, as our galaxies are) H α is about 5–10 times brighter than [O II]. The SFR obtained with this method is uncertain by a factor of 5.

However, this relationship might not be valid at high redshift and the SFR may be overestimated by up to a factor of 10 (Jansen et al. 2001; Hicks et al. 2002). Glazebrook et al. (1999) have compared H α and [O II] luminosities in a sample of 13 $z \sim 1$ field galaxies. The median value in the sample is $L_{H\alpha} \sim 2 \times L_{[\text{OII}]}$; in this relation the dust correction is not

applied.

If we use the prescription (Kennicutt 1998):

$$\text{SFR}_{H\alpha} (M_{\odot} \text{ yr}^{-1}) \simeq \frac{L_{H\alpha}}{1.26 \times 10^{41} \text{ erg s}^{-1}} \quad (3)$$

that gives the SFR for a given H α luminosity, and assume a dust correction (see §8.2) for the H α flux of $A_{H\alpha} = 0.5$ magnitudes (also adopted by Glazebrook et al. 1999), we obtain:

$$\text{SFR}_{[\text{OII}]} (M_{\odot} \text{ yr}^{-1}) \simeq \frac{L_{[\text{OII}]}}{0.39 \times 10^{41} \text{ erg s}^{-1}}, \quad (4)$$

where the [O II] luminosity is the one observed, i.e. not corrected for dust. From this, we derive SFRs in our sample in the range $13-106 M_{\odot} \text{ yr}^{-1}$ (Table 1), with mean and median value of $\sim 40 M_{\odot} \text{ yr}^{-1}$. These values are compared in §8.3, with the SFRs derived using UV luminosities.

High SFR values (derived from Balmer lines) are not new to high redshift star-forming galaxies. For instance, Glazebrook et al. (1999) derived $20-60 M_{\odot} \text{ yr}^{-1}$ in their $z \sim 1$ sample. From UV fluxes, Daddi et al. (2003) derived much higher SFRs in the K20 $1.7 < z < 2.3$ galaxies, with SFRs ranging $100-500 M_{\odot} \text{ yr}^{-1}$. High SFRs are also found in $2.3 \leq z \leq 3.3$ LBGs, for which infrared spectra indicate $\text{SFR} \sim 20-200 M_{\odot} \text{ yr}^{-1}$ (Pettini et al. 1998; Kobulnicky & Koo 2000).

5. CO-ADDITION

In order to improve the signal-to-noise ratio in the 2200–2900 Å spectral range, and to enable studies of the global properties of the galaxy sample, the 13 selected GDDS spectra have been shifted to the rest frame and combined. Both linearly and optimally extracted spectra were initially used and two separate composites have been obtained. To combine the data in a suitable way and maximize the signal-to-noise ratio, we have used the following procedure. The spectra were first normalized to one; this allowed us to analyze in the composite spectrum the EWs of lines of the same ion in a consistent way. The continuum shape was determined by interpolating regions free of spectral features. Then we created for each spectrum a mask spectrum containing “0” or “1”, according to whether the region or pixel can be used or not. Generally, the spectra are relatively free of masked pixels, however small regions in some spectra are contaminated by strong second order refraction. Occasionally other pixels were masked due to strong sky emission line residuals or CCD defects. The total number of masked pixels in the $\lambda = 2200-3000 \text{ Å}$ spectral range is 3.8% of the total.

The observed spectra were shifted to the rest-frame (using ISM redshifts) and linearly averaged to form a mean spectrum (i.e. each galaxy was weighted the same in the composite). The composite noise spectrum is derived consistently. We finally re-normalized the composite spectrum to adjust for misplacements of the continuum in the individual spectra. The uncertainty in the continuum of the composite is estimated to be $\sim 3-5\%$, from the higher to the lower signal regions, and is consistent with the level of the noise per resolution element.

The composite optimal spectrum is shown in Fig. 3 (lower spectrum). For comparison, we also show (shifted upwards along the y-axis) the normalized composite of 14 spectra of local starburst galaxies (Tremonti et al. 2003) obtained with the low resolution Faint Object Spectrograph (FOS) on board of the Hubble Space Telescope (HST). The GDDS mean FWHM in the rest frame is 6.1 Å , and is estimated by considering the observed FWHM divided by $(1 + \langle z \rangle)$, where $\langle z \rangle =$

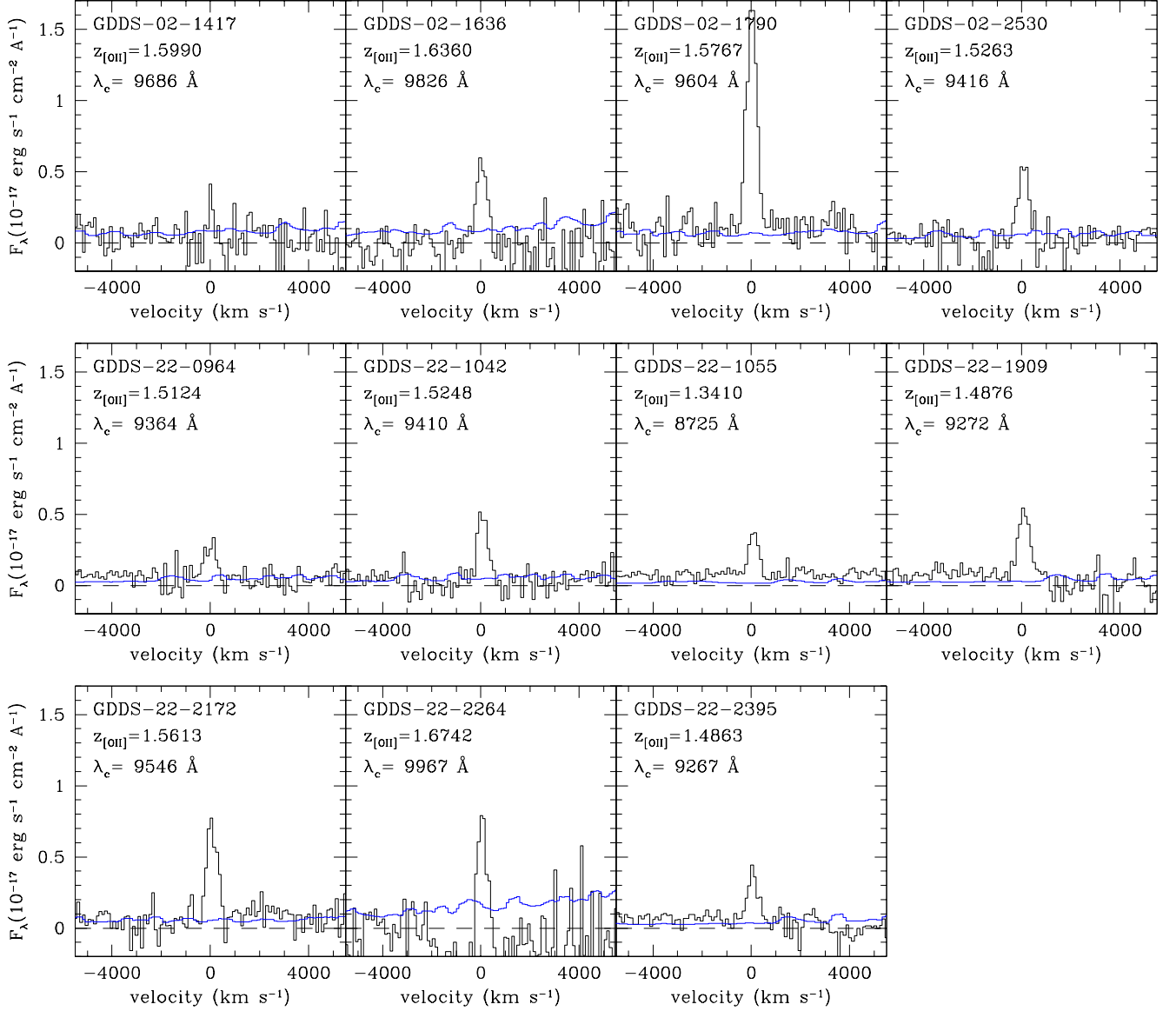


FIG. 2.— [O II] emission for 11 GDDS galaxies. Smooth lines are the noise spectra per pixel ($\sim 3.5 \text{ \AA}$ in the observed frame). Also reported is the central observed [O II] emission line wavelength λ_c . Note that the continuum is not subtracted from the spectra, but subtracted when measuring line fluxes. The flux at $\lambda \sim 9960 \text{ \AA}$ in object GDDS-02-2264 goes below zero due to red-end contamination.

1.60 is the mean redshift of the sample. For the composite we have chosen a small pixel size of 0.7 \AA ($\Delta v \simeq 80 \text{ km s}^{-1}$ at 2600 \AA), i.e. ~ 2 times smaller than the real mean pixel size (1.39 \AA). This allows us to better identify small features in the spectrum and more accurately measure line EWs. The resolution element is extended over ~ 9 pixels. The composite optimal noise spectrum per 0.7 \AA pixel is also shown as a dotted line in Fig. 3.

As a consistency check, the EWs measured from the optimal and linear composite spectra were compared. The agree-

ment is very good and no correlation with, e.g., wavelength is present. Since the signal-to-noise of the optimally extracted composite is 5–15% higher than the linearly extracted one, the optimal composite is used for all subsequent analysis.

The mean S/N per 0.7 \AA pixel in regions free of strong features has been estimated using the noise spectrum. This is $S/N = 9.1$ at $\lambda = 2210\text{--}2330 \text{ \AA}$, $S/N = 12.3$ at $\lambda = 2395\text{--}2570 \text{ \AA}$, $S/N = 14.2$ at $\lambda = 2615\text{--}2785 \text{ \AA}$, $S/N = 11.8$ at $\lambda = 2815\text{--}2990 \text{ \AA}$. The S/N measured with the noise spectrum rescales with the square-root of the pixel size chosen. As a

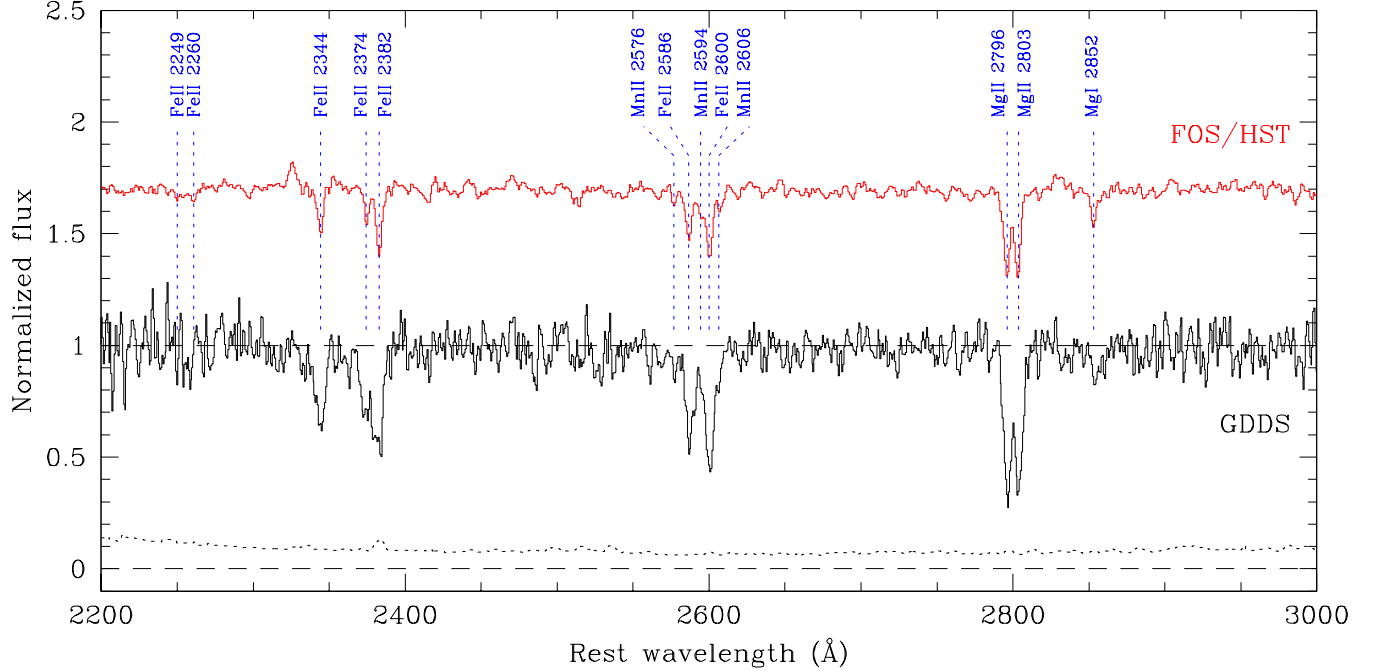


FIG. 3.— Composite spectrum of 13 GDDS galaxies with ISM absorption lines (lower spectrum). The noise per 0.7 \AA pixel (dotted spectrum) is also shown. The sample covers the redshift range $1.34 < z < 1.97$ (mean and median redshift $z = 1.60$ and 1.56 , respectively). Absorption features are also marked. As a reference, we show the composite spectrum of 14 local starburst dwarf galaxies observed with HST/FOS (Tremonti et al. 2003), shifted along the y-axis for comparison.

sanity check, we also measured the standard deviation directly in the signal spectrum. We obtain $S/N = 11.2, 13.6, 18.3$, and 13.9 , in the same regions as before, i.e. about 1.2 times higher than that obtained from the noise spectrum. This is close to the expected value, $\sqrt{2} \simeq 1.4$, given that the chosen pixel size (0.7 \AA) is ~ 2 smaller than the real pixel size (1.39 \AA).

6. HEAVY ELEMENT ENRICHMENT

The ultimate goal of the present analysis is to estimate the heavy element enrichment of galaxies in the GDDS composite spectrum. In the observed range, we have clearly detected Fe II, Mg II and Mg I absorption lines (Fig. 3). Besides these, we have also included in the analysis the very weak Mn II triplet around 2600 \AA . All EWs with errors in the GDDS composite are reported in the third column of Table 2. The 4σ EW upper limits for two Fe II non-detections are also estimated using the noise spectrum, by assuming that lines are extended over 6 \AA (or $\Delta v \sim 800 \text{ km s}^{-1}$ at $\lambda \sim 2250 \text{ \AA}$). Values in brackets are EWs obtained by extrapolating from estimated column densities, see § 6.1. To check the line de-blending in the Fe II $\lambda\lambda 2374, 2382$ and Mg II $\lambda\lambda 2796, 2803$ doublets, we compared the measured EWs in the spectrum with the EWs given by the fit of two blended Gaussians. For the Fe II doublet we measure a ratio between the two lines of 0.59, to be compared with 0.64 given by the ratio of the two Gaussians. For the Mg II doublet we obtain 1.05, to be compared with 1.03 given by the two Gaussians. This shows that the contamination is properly accounted for. The contamination of the Fe II $\lambda 2600$ line by Mn II is treated separately (see next section).

The UV continuum of star-forming galaxies (like our selected sample) is dominated by O and B stars. In this case, the

stellar contamination to the ISM lines in the $2200\text{--}3000 \text{ \AA}$ interval is negligible (Tremonti et al. 2003). Moreover, when stellar wind is not important (this is the case for lines in the $2000\text{--}3000 \text{ \AA}$ region) the strength of the photospheric lines is significantly weaker when compared to ISM lines (de Mello, Leitherer, & Heckman 2000).

The lines detected in the GDDS composite are strong, but narrow in velocity space ($\Delta v < 800 \text{ km s}^{-1}$). Assuming that these interstellar lines originate in gas viewed against the continuum provided by the integrated light of O and B stars in the galaxies, we can measure a sort of “average” column densities of the ions. Two approaches have been followed. In the first case we used EWs as given in Table 2 with the curve of growth analysis (COG, Spitzer 1978). In the second, we simultaneously fit absorption profiles to all lines in the spectrum arising from transitions of the same ion. The advantage of fitting line profiles is that line blending is automatically taken into account.

6.1. Column densities

The rest-frame EWs of the ISM lines detected in the GDDS composite galaxy are very high, indicating that the gas is heavily enriched by metals. As the majority of absorption lines are very strong ($W_r > 1 \text{ \AA}$), they deviate from the linear part of the COG and it is not possible to use the linear approximation to determine column densities. Moreover, the low resolution ($\text{FWHM} \sim 700 \text{ km s}^{-1}$ at $\lambda \sim 2600 \text{ \AA}$) does not allow application of the apparent optical depth method (Savage & Sembach 1991). However, even with the relatively large uncertainties, the general COG analysis can still give significant results since so many lines are present. Given that several galaxy spectra are combined together, it is not pos-

TABLE 2
REST-FRAME EQUIVALENT WIDTHS

| Line | f_λ | W_r (Å) | | |
|----------------------|-------------|-------------------|-------------------|-------------------|
| | | GDDS | cB58 ^a | LBGs ^b |
| Si II λ 1260 | 1.0070 | ... | (2.54 ± 0.07) | < 1.7 |
| Si II λ 1526 | 0.1270 | ... | 2.59 ± 0.03 | 1.72 ± 0.18 |
| Si II λ 1808 | 0.00218 | ... | 0.53 ± 0.02 | $(0.04 - 0.28)$ |
| Fe II λ 1608 | 0.058 | (1.62 ± 0.12) | 1.30 ± 0.04 | 0.91 ± 0.15 |
| Fe II λ 2249 | 0.00182 | < 1.2 | (0.15 ± 0.01) | $(0.048 - 0.13)$ |
| Fe II λ 2260 | 0.00244 | < 0.9 | (0.19 ± 0.01) | $(0.065 - 0.18)$ |
| Fe II λ 2344 | 0.114 | 2.90 ± 0.27 | 2.99 ± 0.04 | ... |
| Fe II λ 2374 | 0.0313 | 2.28 ± 0.23 | 1.94^c | $(0.9 - 1.4)$ |
| Fe II λ 2382 | 0.320 | 3.57 ± 0.31 | 3.41^d | ... |
| Fe II λ 2586 | 0.0691 | 2.96 ± 0.17 | (2.88 ± 0.06) | ... |
| Fe II λ 2600 | 0.239 | 3.94 ± 0.27 | (3.95 ± 0.10) | ... |
| Mn II λ 2576 | 0.3508 | 0.56 ± 0.13 | 0.38 ± 0.10 | ... |
| Mn II λ 2594 | 0.2710 | (0.45 ± 0.16) | (0.30 ± 0.09) | ... |
| Mn II λ 2606 | 0.1927 | (0.33 ± 0.12) | (0.22 ± 0.06) | ... |
| Mg II λ 2796 | 0.6123 | 4.10 ± 0.19 | ... | ... |
| Mg II λ 2803 | 0.3054 | 3.98 ± 0.16 | ... | ... |
| Mg I λ 2852 | 1.8100 | 0.91 ± 0.19 | ... | ... |

NOTE. – Oscillator strengths f_λ are taken from a recent compilation by Prochaska et al. (2001). EWs between brackets are extrapolated from measured column densities (see text). EW upper limits for Fe II in GDDS composite are 4σ .

^aEWs taken from Pettini et al. (2002).

^bEWs taken from Shapley et al. (2003).

^cThe 1σ error reported by Pettini et al. (2002) is > 0.07 Å (line is affected by bad pixels).

^dThe 1σ error reported by Pettini et al. (2002) is > 0.05 Å (line is affected by bad pixels).

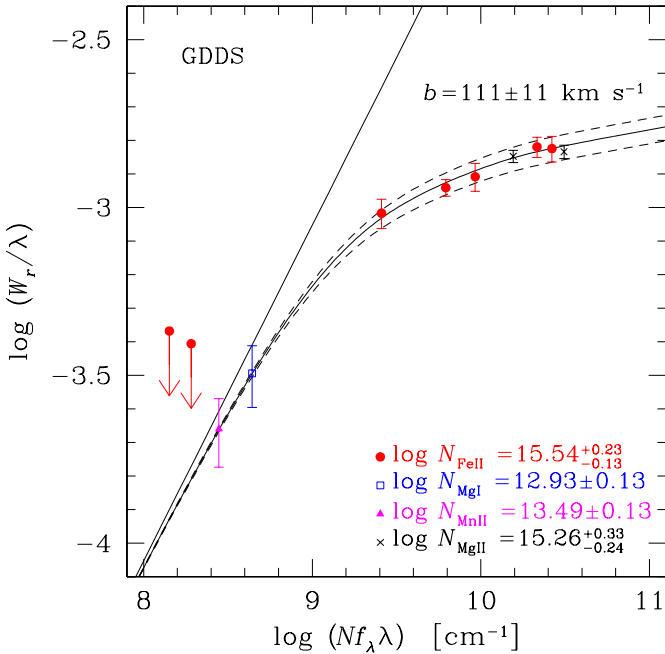


FIG. 4.— Best fit curve of growth for Fe II in the GDDS composite spectrum. The solid and dashed lines are for the best fit Doppler parameter and $\pm 1\sigma$, respectively. The other ion column densities are calculated assuming the best fit b value found for Fe II. The straight line shows the linear approximation to the curve of growth ($b = +\infty$).

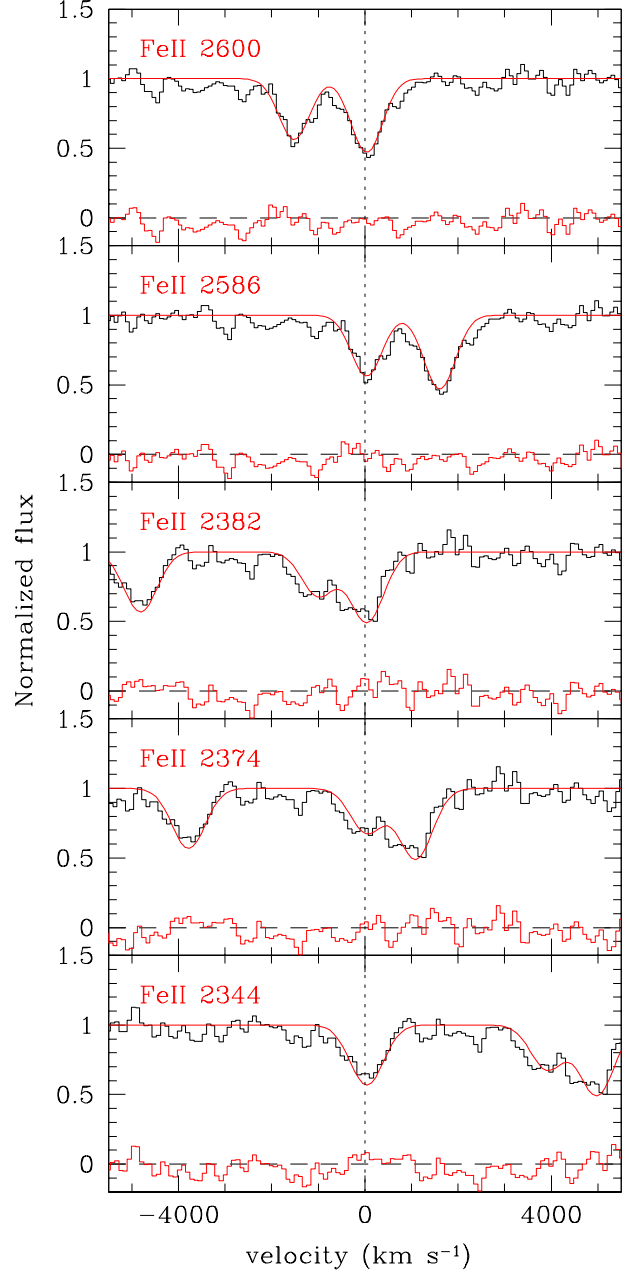


FIG. 5.— Line absorption fitting profile of Fe II for GDDS composite. The smooth line is the best fit with $\log N_{\text{FeII}} = 15.52^{+0.15}_{-0.12}$ and $b = 115 \pm 10$ km s⁻¹. Shown at the bottom are the best fit residuals.

sible to separate the different components of very complex absorption features and therefore they appear as single lines (Fig. 3). Hence, the widths of these features do not provide useful information on the kinematics or thermal conditions of the gas in the galaxies and the broadening is a sort of “effective” Doppler parameter, being the result of the superposition of many absorbing clouds. The COG analysis with a single component approximation was used for QSO-DLA studies before high resolution spectroscopy of QSOs became possible (see for instance Blades et al. 1982; Turnshek et al. 1989; Steidel 1990). In fact, Jenkins (1986) showed that the COG technique applied to complex features nearly always gives a reasonable answer (the simulated-to-true column density ra-

tio rarely goes below 0.8) even if different lines have very different saturation levels or Doppler parameters. The general results have been confirmed by Savage & Sembach (1991), who in addition, show that the COG works best if the gas absorption is not “bimodal” – e.g., that very large absorptions are not combined with narrow ones. Since our composite spectrum is derived from many galaxies, each with many absorption clouds, a bimodal distribution of absorption lines is very unlikely.

In Fig. 4 we show the COG for the absorption lines of the GDDS composite spectrum. The fit to the data was determined by χ^2 minimization of the COG. The resulting column densities are reported in Table 3. To determine the Fe II column density, we have used 5 strong detections, and iterated the results with those for Mn II, because two of the three weak Mn II lines are blended with the Fe II $\lambda 2600$ line. The weakest Fe II line detected, Fe II $\lambda 2374$, gives $\log N_{\text{FeII}} > 15.2$, using the linear approximation for the COG. The non-detection of Fe II $\lambda 2260$ line sets an upper limit of $\log N_{\text{FeII}} < 16$. These two limits already give a good, robust estimate of the Fe II column density. The 5 Fe II EWs give a best fit column density of $\log N_{\text{FeII}} = 15.54^{+0.23}_{-0.13}$, and an effective Doppler parameter $b = 111 \pm 11 \text{ km s}^{-1}$. From this, we extrapolate the EW of the Fe II $\lambda 1608$ line to be $W_r = 1.62 \pm 0.12 \text{ \AA}$. The reduced χ^2 value obtained from the best fit is 0.34, indicating that the errors are probably not underestimated. The Mn II $\lambda 2576$ line is isolated and marginally detected with 4.4σ significance (Table 2). Moreover, the presence of the Mn II absorption is supported by the large EW of the Fe II $\lambda 2600$ line, indicating the presence of Mn II $\lambda \lambda 2594, 2606$ there too. The column density derived from the Mn II $\lambda 2576$ line is in the range $13.25 < \log N_{\text{MnII}} < 13.67$, assuming $b > 90 \text{ km s}^{-1}$, with very little saturation. Taking the same b value as found for Fe II, we find a best fit $\log N_{\text{MnII}} = 13.49 \pm 0.13$. From this, we derive $W_r = 0.45 \pm 0.12 \text{ \AA}$ and $0.33 \pm 0.10 \text{ \AA}$, for Mn II $\lambda 2594$ and Mn II $\lambda 2606$, respectively. These two values have been subtracted from the Fe II $\lambda 2600$ EW and the error propagated. The weak Mg I $\lambda 2852$ line gives $\log N_{\text{MgI}} = 12.93 \pm 0.13$ for $b = 111 \text{ km s}^{-1}$. The Mg II doublet is heavily saturated, namely $\log N_{\text{MgII}} > 14.3$. We estimated $\log N_{\text{MgII}} = 15.26^{+0.33}_{-0.24}$ for a Doppler parameter $b = 111 \pm 11 \text{ km s}^{-1}$ (as for the Fe II best fit).

As a further test on the Fe II column density measurement, we have performed simultaneous line profile fitting of the 5 lines. The result with one component gives $\log N_{\text{FeII}} = 15.52^{+0.15}_{-0.12}$ and $b = 115 \pm 10 \text{ km s}^{-1}$ (Fig. 5), very similar to that found with the COG method ($\log N_{\text{FeII}} = 15.54^{+0.23}_{-0.13}$), with a reduced $\chi^2 = 0.55$. This shows consistency between the line profiles and the column density derived using the COG. The velocity shift between the fit and the rest frame is consistent with zero.

We finally considered another source of uncertainty: the ISM covering factor. So far we assumed that the covering factor is one, that is the gas is uniformly distributed in front of the emitting sources, and photons escaping the absorbing gas or scattered are not important. However, in case of a non-unity covering factor, the residual flux not absorbed by the ISM would cause a systematic underestimate of the column densities, if not properly taken into account. From the depth of the MgII absorption, we have estimated that the covering factor is at least 70%. We recalculated the FeII column density, assuming this very conservative lower limit, and obtained

$N_{\text{FeII}} \sim 60\%$ higher than in the case of unity covering factor. In log scale the difference is only 0.2 dex: $\log N_{\text{FeII}} = 15.75$ instead of $\log N_{\text{FeII}} = 15.54$; this is within the upper error estimated in our first measurement (0.23 dex). Shapley et al. (2003) discuss the non-unity of the covering factor in LBGs. However, Giallongo et al. (2002) found that in two LBGs the escaping fraction of ionizing photons ($\lambda < 912 \text{ \AA}$) is $< 16\%$, whereas Malkan, Webb & Konopacky (2003) found that the same quantity in the UV images of 11 bright blue $1.1 < z < 1.4$ galaxies is less than 6%. Both results evoke some caution on this issue.

7. METAL COLUMN DENSITIES IN HIGH REDSHIFT ISM

When the gas is mostly neutral ($N_{\text{HI}} \sim N_{\text{H}}$), the column density of an element can be approximated with the column density of the ion with ionization potential above the hydrogen ionization potential (13.6 eV). For instance, iron, magnesium and manganese are mainly in the Fe^+ , Mg^+ , and Mn^+ state. In the GDDS composite, the very high EWs of Fe II and Mg II indicates that the gas is nearly neutral and the $N_{\text{FeII}} \sim N_{\text{Fe}}$, $N_{\text{MgII}} \sim N_{\text{Mg}}$, or $N_{\text{MnII}} \sim N_{\text{Mn}}$ approximation can be applied. The low ionization of the gas is confirmed by the presence of a relatively strong Mg I absorption ($\log N_{\text{MgI}} \sim 12.9$), but with column density much lower than the Mg II column density ($\log N_{\text{MgII}} \sim 15 - 15.6$).

Considering column densities of these ions in the neutral ISM instead of metallicities (element-to-hydrogen relative abundance) has the advantage that we can directly compare results with other classes of objects at various redshifts with similar measurements, without knowing the H I content. Indeed, H I absorption in GDDS spectra cannot be detected for lack of spectral coverage. In Table 3 we compare column densities of Fe II, Mn II, Si II, observed in the GDDS composite, and other high redshift and local galaxies.

Heavy element column densities in the neutral ISM of high redshift galaxies have been measured in great detail for more than 100 QSO-DLAs in the interval $0.0 < z < 4.5$ (see for instance Lu et al. 1996; Pettini et al. 1997; Prochaska & Wolfe 1999; Prochaska et al. 2003a). For our purpose, we have used our own large compilation of DLAs¹⁸. The mean column densities for Fe II, Mn II, and Si II with dispersions are given in Table 3. We have divided the sample in subsamples for each ion. The number of DLAs considered in each subsample is also given in the first column (between brackets). The column density distributions for Fe II and Mn II as a function of redshift are shown in Figs. 7 and 8.

The heavy element column densities in the ISM of GRB-DLAs have been studied in only 4 objects (Savaglio et al. 2003, Vreeswijk et al. 2003). In a fifth event, GRB 020813 ($z = 1.255$), equivalent widths of many UV lines have been reported by Barth et al. (2003), from which we have estimated column densities using the COG (Table 3).

We also include in our analysis, the ISM lines measured in star-forming galaxies in the local Universe observed with the Far Ultraviolet Spectroscopic Explorer (FUSE). The sensitivity and resolution ($\text{FWHM} \sim 30 \text{ km s}^{-1}$) of FUSE is good enough for a detailed analysis of nearby starburst galaxies. In our study we considered metal column densities obtained for NGC 1705 (Heckman et al. 2001) and I Zw 18 (Aloisi et al. 2003). For comparison, we have also included measurements in the diffuse and dense ISM of the Milky Way and

¹⁸ For the largest public compilation of DLA column densities, visit J. Prochaska’s homepage at <http://www.uchicago.edu/~xavier/ESI>.

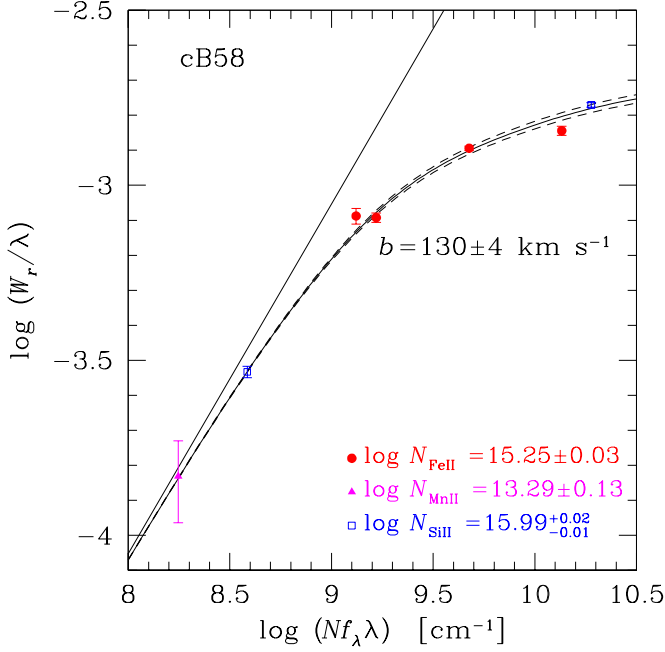


FIG. 6.— Best fit curve of growth for Fe II in the cB58 ISM. The solid and dashed lines are for the best fit Doppler parameter and $\pm 1\sigma$, respectively. The Mn II column density is calculated assuming the best fit b value found for Fe II. The best fit for Si II is calculated independently and is not shown for clarity, but this is very similar to the Fe II best fit. The straight line shows the linear approximation to the curve of growth ($b = +\infty$).

the Magellanic Clouds (Sembach & Savage 1996; Spitzer & Fitzpatrick 1995; Welty et al. 1997, 1999).

The neutral ISM metal enrichment of LBGs has been discussed by Shapley et al. (2003) for a composite of 811 spectra, and by Pettini et al. (2002) for the bright LBG galaxy cB58 at $z = 2.72$. In the following sections, we use their EWs and estimate heavy element column densities using the COG.

7.1. The spectrum of the LBG MS 1512–cB58

Column densities in the LBG MS 1512–cB58 ($z = 2.72$) have been determined by Pettini et al. (2002) using the apparent optical depth (Savage & Sembach 1991) measured on the less saturated lines. For a comparison of the COG with this method, we have redone the analysis for cB58 using the COG. The EWs used are given in the fourth column of Table 2 and are the ones reported by Pettini et al. (2002). The COG for cB58 is shown in Fig. 6 and the column densities are listed in Table 3. The EWs of two of the four Fe II lines, Fe II $\lambda\lambda 2374, 2382$, have errors larger than 0.07 and 0.05 Å for contamination by bad pixels (Pettini et al. 2002), for which we arbitrarily use $\sigma = 0.15$ Å.

The advantage of using the COG is that all detected Fe II lines can be used, regardless of the saturation level. The apparent optical depth method, as Pettini et al. (2002) points out, can still underestimate column densities due to saturation. This effect is also noted in the ISM of local dwarf galaxy I Zw 18 by Aloisi et al. (2003), who made a comparison between the line fitting of Voigt profiles and the apparent optical depth method. The COG analysis for cB58 is shown in Fig. 6. The best fit to the four Fe II lines gives $\log N_{\text{FeII}} = 15.25^{+0.04}_{-0.03}$ and $b = 130 \pm 4 \text{ km s}^{-1}$ ($\chi^2 = 3.9$), consistent with $\log N_{\text{FeII}} \simeq 15.20$ found by Pettini et al. (2002).

Errors on column densities derived by Pettini et al. (2002) are reported to be generally less than 0.2 dex.

The Mn II $\lambda 2576$ line is very close to the linear part of the COG, therefore the column density is relatively well constrained in the range $\log N_{\text{MnII}} = 13.12 - 13.44$ for $b > 90 \text{ km s}^{-1}$. If we adopt $b = 130 \text{ km s}^{-1}$, as given by Fe II, we obtain $\log N_{\text{MnII}} = 13.29 \pm 0.13$, consistent with $\log N_{\text{MnII}} \simeq 13.33$ found by Pettini et al. (2002). From this column density and Doppler parameter, we derived the expected EWs of the Mn II $\lambda\lambda 2594, 2607$ doublet (Table 2).

For completeness, we also estimate the Si II column density. Si II $\lambda 1260$ is weakly contaminated by S II $\lambda 1259$ and Fe II $\lambda 1260$ ($W_r \sim 1$ Å), therefore we do not use it. The other two detected lines have very different oscillator strengths. The Si II $\lambda 1808$ line is weak and little saturated, and gives a column density in the range $15.92 < \log N_{\text{SiII}} < 16.05$ for $b > 70 \text{ km s}^{-1}$. From Si II $\lambda\lambda 1526, 1808$ together, we derive $\log N_{\text{SiII}} = 15.99^{+0.01}_{-0.02}$ and $b = 136 \pm 2 \text{ km s}^{-1}$, consistent with $\log N_{\text{SiII}} \simeq 15.99$ given by Pettini et al. (2002). We also note that the effective Doppler parameter for Fe II and Si II have been found independently to be very similar ($b_{\text{FeII}} = 130 \text{ km s}^{-1}$ and $b_{\text{SiII}} = 136 \text{ km s}^{-1}$).

We found an excellent agreement between the results obtained by Pettini et al. (2002) using the apparent optical depth method and ours obtained with the COG (Table 3), supporting the robustness of our results for GDDS galaxies.

7.2. The LBG composite spectrum

Shapley et al. (2003) have used 811 LBG spectra in the redshift range $2 < z < 3.8$ to construct a UV ($\lambda = 950 - 1850$ Å) composite spectrum. Their composite is rather complex, showing stellar features, low and high ionization absorption, and nebular emission lines. EWs of ISM lines are reported, but column densities are not derived because lines are heavily saturated. They also subdivided the sample into 4 subsamples according to the Ly α equivalent width, in order to find possible correlation with observed parameters. Here we only consider the EWs of the total composite. Although the few ISM lines are saturated ($W_r > 0.9$ Å), inspecting them with the COG can provide interesting, even if qualitative, results on the heavy element enrichment in the neutral ISM. We assume that the covering factor of the ISM in front of the UV sources is one. If the covering factor is less than one, column densities derived using the COG would be systematically lower than real values.

Only Fe II $\lambda 1608$ is measured for Fe II, but because this line is moderately saturated, it can be used to constraint the column density. We derive $14.76 < \log N_{\text{FeII}} < 15.21$, assuming an effective Doppler parameter $b > 90 \text{ km s}^{-1}$ (a reasonable assumption given that 811 galaxy spectra are coadded). From this, we derive the expected EWs for other Fe II transitions (between brackets in Table 2). The Si II $\lambda 1304$ line is contaminated by O I $\lambda 1302$, while Si II $\lambda 1260$ is contaminated by S II $\lambda 1259$ and Fe II $\lambda 1260$. To determine the Si II column density, we used these two EWs as upper limits and in addition the Si II $\lambda 1526$ measurement. Assuming $b > 90 \text{ km s}^{-1}$, we get $\log N_{\text{SiII}} = 14.8 - 15.7$, from which we expect $W_r(\text{Si II } \lambda 1808) = 0.04 - 0.28$ Å (Table 2).

A comparison between the GDDS composite and the LBG composite can be made by considering the Fe II $\lambda 1608$ line. Given the good accuracy of our Fe II column density measurement, we can estimate the expected EW for the Fe II $\lambda 1608$ line (that is not covered by our data), and get $W_r = 1.6 \pm 0.2$

TABLE 3
INTERSTELLAR COLUMN DENSITIES

| Galaxy | redshift | $\log N \text{ (cm}^{-2}\text{)}$ | | | | Ref |
|-----------------------------|-----------|-----------------------------------|--------------------------|--------------------------|--------------------------|-------|
| | | Fe II | Mn II | Si II | H I | |
| GDDS (13) | 1.60 | $15.54^{+0.23}_{-0.13}$ | 13.49 ± 0.13 | ... | ... | 1 |
| MW–MC | 0.00 | $\langle 14.89 \rangle$ | $\langle 13.00 \rangle$ | $\langle 15.53 \rangle$ | ... | 2,3,4 |
| I Zw 18 | 0.0026 | 15.09 ± 0.06 | ... | 14.81 ± 0.07 | 21.34 ± 0.11 | 5 |
| NGC 1705 | 0.0021 | 14.54 ± 0.10 | ... | 14.61 ± 0.14 | 20.2 ± 0.2 | 6 |
| GRB 990123 | 1.6004 | $14.78^{+0.17}_{-0.10}$ | ... | ... | ... | 7 |
| GRB 000926 ^a | 2.038 | $15.60^{+0.20}_{-0.15}$ | ... | $16.47^{+0.10}_{-0.15}$ | ~ 21.3 | 7 |
| GRB 010222 | 1.475 | $15.32^{+0.13}_{-0.10}$ | $13.61^{+0.08}_{-0.06}$ | 16.09 ± 0.05 | ... | 7 |
| GRB 020813 ^b | 1.255 | $15.52^{+0.02}_{-0.03}$ | 13.63 ± 0.02 | 16.28 ± 0.03 | ... | 1 |
| GRB 030323 | 3.3714 | 15.93 ± 0.08 | ... | ... | 21.90 ± 0.07 | 8 |
| cB58 ^c | 2.72 | $15.25^{+0.04}_{-0.03}$ | 13.29 ± 0.13 | $15.99^{+0.01}_{-0.02}$ | 20.85 ± 0.09 | 9 |
| LBGs (811) ^c | ~ 3 | $14.8 - 15.2$ | ... | $14.8 - 15.7$ | ... | 10 |
| QSO–DLAs (120) ^d | 0.56–4.47 | 14.39 (0.62)^e | ... | ... | 20.60 (0.51)^e | 11 |
| QSO–DLAs (21) ^d | 0.56–2.78 | ... | 12.68 (0.44)^e | ... | 20.68 (0.56)^e | 11 |
| QSO–DLAs (105) ^d | 0.68–4.47 | ... | ... | 14.71 (0.70)^e | 20.52 (0.50)^e | 11 |

References. – (1) This work; (2) Sembach & Savage (1996); (3) Spitzer & Fitzpatrick (1995); (4) Welty et al. (1997, 1999); (5) Aloisi et al. (2003); (6) Heckman et al. (2001); (7) Savaglio et al. (2003); (8) Vreeswijk et al. 2003; (9) Pettini et al. (2002); (10) Shapley et al. (2003); (11) Obtained from a compilation of QSO–DLAs

^aH I column density estimated by Fynbo et al. 2002.

^bLine EWs are taken from Barth et al. 2003.

^cWe have estimated column densities using the COG.

^dIn brackets is the number of QSO–DLAs used.

^eIn brackets is the dispersion in the sample.

Å (Table 2). This is 1.8 times higher than the EW of the same line measured by Shapley et al. (2003) in the LBG composite ($W_r = 0.91 \pm 0.15$ Å), but it is similar to that of the LBG subset (1/3 of the galaxies) that does not display Ly α emission ($W_r = 1.57 \pm 0.21$ Å).

8. DISCUSSION

Various methods have been traditionally used to derive metallicities in high redshift galaxies using both absorption and emission lines. The Lick indices method (Faber et al. 1985), recently applied on SDSS $0.15 < z < 0.50$ galaxies (Eisenstein et al. 2003), compares absorption line strengths in stars with models (Vazdekis 1999) and is mostly sensitive to old stellar population systems. As Eisenstein et al. (2003) point out, the models are limited in the range of metallicities and can suffer from the age–metallicity degeneracy.

Nebular emission in the ionized ISM is, on the other hand, more appropriate when dealing with star-forming galaxies. The metallicity, measured using [O II] $\lambda 3727$, [O III] $\lambda \lambda 4959, 5007$, and Balmer emission lines of 56 galaxies at $0.26 < z < 0.86$, ranges from half to two times solar (Kobulnicky et al. 2003). In a similar study (66 galaxies at $0.5 < z < 0.9$) Lilly, Carollo & Stockman (2003) find that most galaxies in their sample have $Z \sim Z_\odot$. This method relies on a good calibration of metallicity vs. line strengths derived from samples in the local Universe, and requires also a reliable estimate of the stellar Balmer absorption line contamination. As Kobulnicky et al. (2003) mention, it is useful in a statistical sense when using large data sets. Moreover, this method requires IR spectroscopy for galaxies at $z > 0.8$.

In our first analysis of GDDS data, we used UV absorption lines associated with the neutral ISM to evaluate heavy element enrichment in a subset of galaxies in $1.34 < z < 1.97$. This sample represents a joint set of the most massive galaxies at $z > 1.3$ (from the deep K selection) together with those with the strongest rest-frame UV emission (from the M_{2000} selection). Thus we are selecting massive starburst galaxies; preliminary stellar mass estimates (Glazebrook et al. in preparation) indicate that they have masses $M \gtrsim 10^{10} M_\odot$ and their descendants must correspond to galaxies of at least this mass today. This selection is quite similar to that of Lilly et al. (2003) at $z \sim 0.7$ whose primary I -band selection pulls out massive galaxies and whose emission line cut pulls out a high-SFR subset.

8.1. Metal content at high redshift

One of the advantages of using ISM absorption lines associated with singly ionized elements in galaxies is that no model-dependent assumptions or calibrations, dust extinction or ionization corrections are important when deriving the heavy element enrichment.

In Fig. 7 we show the Fe II column density measured in the ISM of different galaxies, as a function of redshift. In our analysis we unambiguously find that the metal enrichment of the GDDS galaxies is high, with $\log N_{\text{FeII}} = 15.54^{+0.23}_{-0.13}$. Eighteen QSO–DLAs have measured Fe II column density in the same redshift range ($1.34 < z < 1.97$). In this sample the highest column density of Fe II is $\log N_{\text{FeII}} \simeq 15.36$, i.e. ~ 1.5 times lower than in the GDDS composite. If we extend the range to $1.0 < z < 2.0$, we find 24 QSO–DLAs, and 2 systems

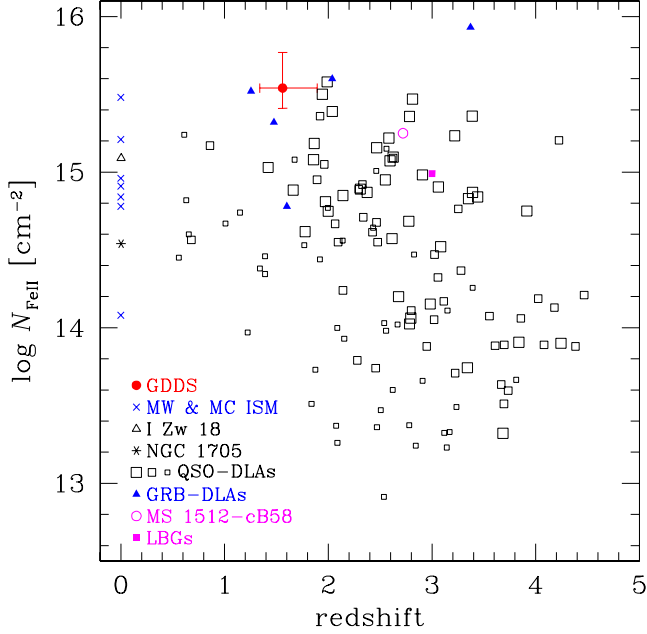


FIG. 7.— Fe II column densities as a function of redshifts in different galaxies. QSO-DLAs are divided in three subsamples where small, medium and big squares indicate $\log N_{\text{HI}} < 20.45$, $20.45 < \log N_{\text{HI}} < 20.80$, and $\log N_{\text{HI}} > 20.80$ systems, respectively. Errors for $\log N_{\text{FeII}}$ in QSO-DLAs is always < 0.2 dex, and on average is 0.05 dex. Errors for local ISM column densities, when available, are typically less than 0.1 dex. For $\log N_{\text{FeII}}$ in the LBGs, we have taken the middle point in the interval $\log N_{\text{FeII}} = 14.76 - 15.21$. Errors on the other column densities are given in Table 3.

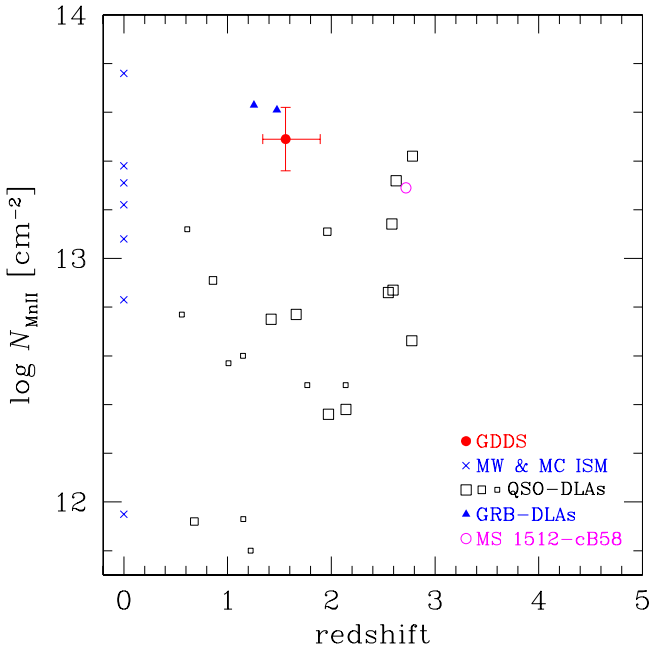


FIG. 8.— As in Fig. 7, but for Mn II column densities. The error for $\log N_{\text{MnII}}$ in QSO-DLAs is on average 0.07 dex. Errors for local ISM column densities, when available, are typically less than 0.1 dex.

with comparable column density (8% of the total, or 15% if only $\log N_{\text{HI}} \geq 20.3$ systems are considered). This is still a significant difference with the GDDS composite. On the other hand, high values of Fe II column density are found in other star-forming galaxies: the GRB host galaxies, and the LBGs cB58 at $z = 2.72$ (Table 3).

We note that when the background source is external to the galaxy (as for QSO-DLAs) the column density of an ion is higher than when the background source is inside the galaxy (as for the GDDS composite). In the former case, the line of sight crosses the entire galaxy, whereas in the latter only the gas in front of the stars is probed. The simplest situation would be that the stars are at the center, therefore the observed column is a factor of 2 less than what a background QSO would see. For some distribution of stars and gas, the correction could be larger or smaller, but never downward. This would reinforce our findings of high Fe II column density in GDDS galaxies with respect to typical Fe II column densities in QSO-DLAs.

Similarly, in Fig. 8 we show the Mn II column densities in the ISM of different galaxies. Even if the number of detections is much lower, the trend shown by Fe II is confirmed. In the whole QSO-DLA sample, only two (out of 21, 9.5%, or 13% if $\log N_{\text{HI}} \geq 20.3$ systems only are considered) have Mn II column density comparable to the GDDS composite ($\log N_{\text{MnII}} = 13.49 \pm 0.13$). At $1 < z < 2$, all 9 QSO-DLAs with detected Mn II have $\log N_{\text{MnII}} \leq 13.1$. Comparable values are found, once again, in GRB host galaxies and cB58 (Table 3).

The Mg II doublet is very strong in the GDDS composite (Fig. 3), but is highly saturated and the column density very uncertain ($\log N_{\text{MgII}} = 15.26^{+0.33}_{-0.24}$). From this, we derive a magnesium-to-iron relative abundance¹⁹ in the range $-0.84 < [\text{Mg}/\text{Fe}] < 0.13$. In the Galactic ISM, Fe is more depleted in dust than Mg, and $[\text{Mg}/\text{Fe}]$ in the gas form is in the range $0.1 < [\text{Mg}/\text{Fe}] < 0.8$. A smaller content of Fe with respect to Mg is also expected in the case of α -element enhancement (Mg is an α element) in metal poor systems. The low value of $[\text{Fe}/\text{Mg}]$ found in the GDDS composite may also indicate that there is a residual saturation in the measured Mg II column density that is not taken into account.

The Mg II absorption has been extensively studied along QSO sight lines (Rao & Turnshek 2000; Churchill, Vogt, & Charlton 2003; Ding et al. 2003). These absorbing clouds have been claimed to be associated with galaxy environment with $\log N_{\text{HI}} \gtrsim 17.3$. When the EW of the Mg II doublet is less than $\sim 1 \text{ \AA}$, the absorbing gas originates in halo clouds, while for larger EWs, the system is very likely a DLAs (Rao & Turnshek 2000). In GRB afterglows, the Mg II absorption is, when detected, very strong and often used to identify the redshift, since it can be detected in the optical up to $z \sim 2.2$. In Fig. 9 we show the Mg II doublet EWs seen in QSO sight-lines, GRB afterglows, and GDDS composite, as a function of redshift. The difference between QSO sight-line studies and star-forming galaxies is apparent.

Unfortunately for lack of wavelength coverage we have no information on the Ly α absorption in our GDDS spectra. Therefore the H I column density and the metal content relative to hydrogen cannot be derived. A rough estimate of the H I column density can be obtained using the correlation

¹⁹ We adopt the definition $[X/Y] = \log N_X/N_Y - \log(X/Y)_\odot$, where $(X/Y)_\odot$ is the meteoritic solar abundance of element X with respect to element Y as given by Grevesse & Sauval 1998.

between the SFR surface density and the H I surface density, found by Kennicutt (1998) for local disk galaxies. Our slit aperture of 0.75 arcsec corresponds to a physical size (at $z = 1.6$) of 6.4 kpc. The signal along the y direction has been extracted over 9.6 pixels (average value for the 13 galaxies) and this corresponds to 0.70 arcsec, or 5.9 kpc. If we assume that the detected flux comes from a $6.4 \times 5.9 = 37.7 \text{ kpc}^2$ surface, and take the median SFR of the sample $\sim 40 \text{ M}_\odot \text{ yr}^{-1}$ (derived from [O II] emission), we obtain a SFR surface density:

$$\log \Sigma_{\text{SFR}} \simeq 0.02 \text{ M}_\odot \text{ yr}^{-1} \text{ kpc}^{-2} \quad (5)$$

which corresponds to a H I surface density of $\log \Sigma_{\text{HI}} \sim 1.6 \text{ M}_\odot \text{ pc}^{-2}$ (± 0.3 dex dispersion), or to a H I column density $\log N_{\text{HI}} = 21.7 \pm 0.3$. Changing the SFR by 20%, would change the H I of $\sim 10\%$. Taking the Fe II column density determined with the COG ($\log N_{\text{FeII}} = 15.54^{+0.23}_{-0.13}$), and assuming a moderate Fe dust depletion, $\delta_{\text{Fe}} \equiv \log N_{\text{Fe,tot}} - \log N_{\text{Fe,gas}} = 1.0$ dex (similar depletions are found in Galactic warm disk and halo+disk gas clouds; Savage & Sembach 1996), we obtain a metallicity $Z/Z_\odot = 0.2^{+0.5}_{-0.1}$. The error includes 20% and 0.2 dex dispersion in the SFR and dust depletion, respectively, as well as the uncertainty in the H I and Fe II column densities.

The median H I column density for 135 QSO-DLAs with $\log N_{\text{HI}} \geq 20.3$ is $\log N_{\text{HI}} \simeq 20.7$. About 1/4 of these have $\log N_{\text{HI}} \geq 21.0$ and none has $\log N_{\text{HI}} > 21.85$. For the LBG cB58 a $\log N_{\text{HI}} \simeq 20.9$ have been reported (Savaglio et al. 2002; Pettini et al 2002). To date, this is the only LBG for which the H I column density has been measured. High H I column densities have also been estimated in GRB 000926 and GRB 030323 (Table 3). In addition, for GRB 000301C ($z = 2.040$) and GRB 020124 ($z = 3.198$) a tentative $\log N_{\text{HI}} \approx 21.2$ and 21.7, respectively, have been reported (Jensen et al. 2001; Hjorth et al. 2003). If we assume for the GDDS composite a H I column density in the range $\log N_{\text{HI}} \sim 21.0 - 21.7$, and apply the same dust correction as before ($\delta_{\text{Fe}} = 1$ dex), we obtain $Z/Z_\odot \sim 1 - 0.2$.

A high metallicity would not be terribly surprising, because even if QSO-DLAs dust-corrected metallicities are on average $\sim 1/10$ solar in the redshift range $1 < z < 2$ (Savaglio 2000; Prochaska et al. 2003b), at redshift $0.3 < z < 0.9$ higher metallicities (0.5 to 2 times solar) have been found in H II regions (Kobulnicki et al. 2003; Lilly et al. 2003). For cB58 at $z = 2.72$ Pettini et al. (2002) report $Z/Z_\odot \sim 2/5$. Heckman et al. (1998) have found that in the local Universe more luminous starbursts have also higher metallicities and are dustier. Similarly, our subsample of GDDS galaxies is selected to be the most luminous in the sample, therefore they could also be the most metal rich.

8.2. Dust depletion and extinction in the gas

The relative abundances of elements with different depletion levels can be used to estimate the dust content in galaxies. For example, Zn is typically hardly depleted in the ISM, while Fe is much more depleted. The zinc-to-iron relative abundance is on average $[\text{Zn}/\text{Fe}] \simeq 0.52$, in 44 QSO-DLAs ($\langle z \rangle = 2.0$) with a 1σ dispersion of 0.28 dex. This is reminiscent of the depletion pattern in the warm halo clouds of the MW, where $[\text{Zn}/\text{Fe}] \sim 0.6$ (Savage & Sembach 1996).

In the GDDS composite, the Zn II doublet is off the wavelength range, whereas Fe II and Mn II were both detected. Unfortunately, both Fe and Mn are strongly affected by the presence of dust (Savage & Sembach 1996). We obtain a very un-

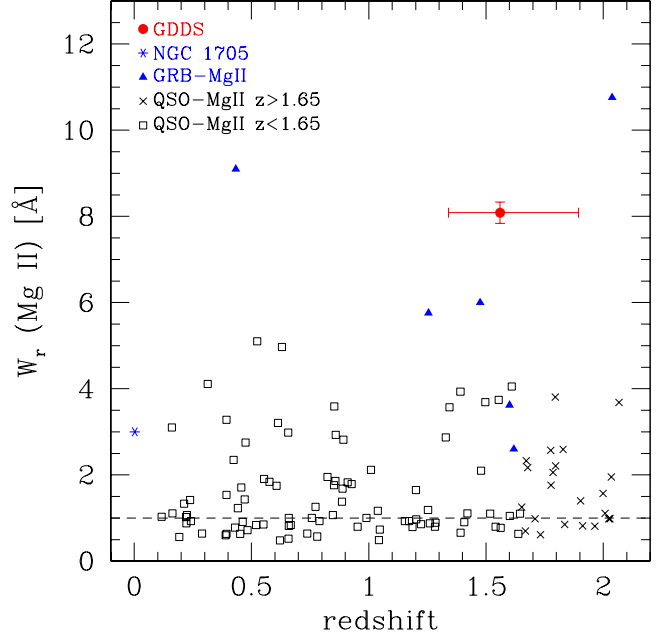


FIG. 9.— Equivalent widths of the Mg II $\lambda\lambda 2796, 2803$ doublet as a function of redshift in GDDS composite galaxy, QSO-Mg II absorbers, GRB afterglows and star-forming galaxy NGC 1705. QSO-Mg II absorbers at $z < 1.65$ and $z > 1.65$ are from Rao & Turnshek (2000) and Steidel & Sargent (1992), respectively. QSO-Mg II systems with total EW larger than $W_r = 1 \text{ \AA}$ (dashed line) are most likely QSO-DLAs. The four GRB detections are from, in order of increasing redshift, GRB 990712 ($z = 0.433$; Vreeswijk et al. 2001), GRB 020813 ($z = 1.255$; Barth et al. 2003), GRB 010222 ($z = 1.475$; Jha et al. 2001; Masetti et al. 2001; Mirabal et al. 2002; Salamañca et al. 2001), GRB 990123 ($z = 1.600$; Kulkarni et al. 1999), GRB 990712 ($z = 1.619$; Vreeswijk et al. 2001) and GRB 000926 ($z = 2.038$; Castro et al. 2003). The EW for NGC 1705 are from Vázquez et al. (in preparation).

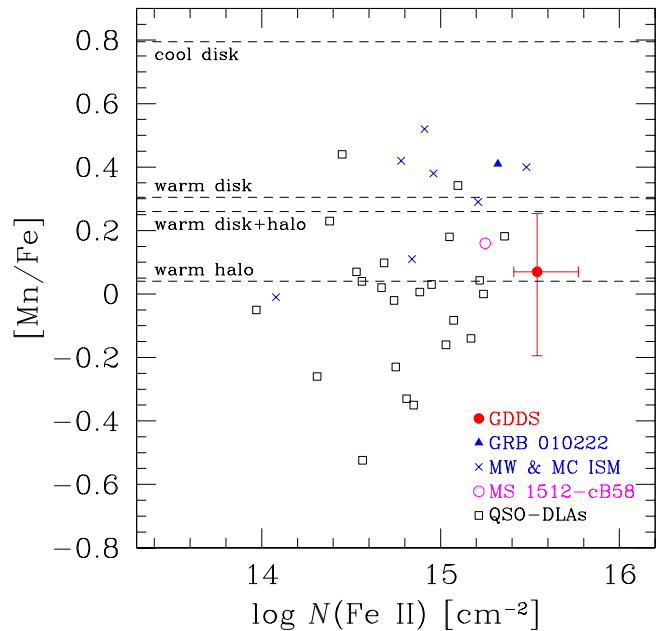


FIG. 10.— Manganese-to-iron relative abundances as a function of Fe II column density in different high redshift galaxies and in the MW and MCs. The dashed lines indicate $[\text{Mn}/\text{Fe}]$ found in, from top to bottom, cool disk, warm disk, warm disk+halo and warm halo clouds of the MW (Savage & Sembach 1996).

certain $[\text{Mn}/\text{Fe}] = 0.07^{+0.18}_{-0.26}$ in the GDDS composite (Fig. 10). Future analysis with more data will allow to constrain better this measurement. In 28 QSO-DLAs with $\langle z \rangle = 1.59$, we found $[\text{Mn}/\text{Fe}] = -0.02$ with 0.22 dex dispersion. In the MW, the depletion patterns found by Savage & Sembach (1996) indicate $[\text{Mn}/\text{Fe}]$ in the range 0.0–0.8, going from warm halo to cool disk clouds. A deficiency of Mn with respect to Fe has been found in low metallicity stars, due to “odd–even” effect in the iron-peak element production. This shows $[\text{Mn}/\text{Fe}] \sim -0.4$ for $[\text{Fe}/\text{H}] < 1$ and a linear increase for $[\text{Fe}/\text{H}] > 1$ up to $[\text{Mn}/\text{Fe}] \sim 0.1$ for $[\text{Fe}/\text{H}] \sim 0.3$ (McWilliam, Rich, & Smecker–Hane 2003).

Independent of the Mn II detection, the effects of dust obscuration can be estimated by assuming that this is proportional to the column density of Fe II. We know that in the solar neighborhood, the optical obscuration due to a gas cloud is (Bohlin, Savage & Drake, 1978):

$$A_V \simeq 0.5 \times \frac{Z}{Z_\odot} \times \frac{N_{\text{HI}}}{10^{21}}. \quad (6)$$

As $ZN_{\text{HI}} \propto N_{\text{FeII}}$, Eq. 6 can be expressed in terms of the Fe II column density in the cloud:

$$A_V \simeq 0.5 \times 10^{\log N_{\text{FeII}} + \delta_{\text{Fe}} - 21 - \log(\text{Fe}/\text{H})_\odot} \quad (7)$$

where $\log(\text{Fe}/\text{H})_\odot = -4.50$ is the solar iron abundance relative to hydrogen. For a Fe dust depletion $\delta_{\text{Fe}} = 1$ dex (similar to the warm disk and warm disk+halo depletion in the MW; Savage & Sembach 1996), and $\log N_{\text{FeII}} = 15.54^{+0.23}_{-0.13}$, we obtain $A_V = 0.6^{+0.4}_{-0.2}$, regardless of the H I column density. At the wavelength of the H α the extinction is ~ 0.5 magnitudes, or a factor of ~ 1.6 in the flux. This is the value used in §4 to derive SFRs from [O II] emission. For $\delta_{\text{Fe}} = 0.6$, like in the MW warm halo clouds, the optical extinction is $A_V = 0.2^{+0.2}_{-0.1}$.

In QSO-DLAs (where iron depletion is on average $\delta_{\text{Fe}} = 0.52 \pm 0.23$) the optical extinction is generally lower ($A_V \lesssim 0.1$), most likely due to an observational bias (Savaglio 2000). This is marginally supported by the work of Ellison et al. (2001), who tentatively found more DLAs in radio-selected QSOs than in optically selected QSOs ($\sim 2\sigma$ significant).

8.3. SFRs from UV luminosities

Independently of the [O II] luminosity, SFRs can be derived using the rest-frame UV luminosities. These are more affected by dust extinction correction than those obtained using [O II]. Moreover, UV emission is less directly connected to the instantaneous star formation, because associated with less massive stars than the nebular emission. However, it is interesting to evaluate SFRs from a completely independent method. The M_{2000} absolute magnitude (Table 1) gives an absolute intrinsic (dust corrected) luminosity:

$$L_{2000} = 4\pi R_{10pc}^2 \times 10^{-19.438 - 0.4(M_{2000} - A_{2000})} \quad (8)$$

where $R_{10pc} = 3.08 \times 10^{19}$ cm, and A_{2000} is the global (in the gas and stars) extinction at 2000 Å. To derive SFRs from UV luminosities, different conversion factors can be used, according to different models that uses different initial mass functions (IMFs) and metallicities. Even if the conversion factor can vary from one model to another, Glazebrook et al. (1999) have shown that the variation is at most within a factor of two. For convenience, we select an intermediate case valid for a solar metallicity and Salpeter IMF. Glazebrook et al. (1999)

gives, for $\text{SFR} = 1 \text{ M}_\odot \text{ yr}^{-1}$, luminosities between 8.7 and $7.2 \times 10^{27} \text{ erg s}^{-1} \text{ Hz}^{-1}$ for the 1500–2800 Å interval. We adopt

$$\text{SFR}_{2000}(\text{M}_\odot \text{ yr}^{-1}) = \frac{L_{2000}}{8 \times 10^{27} \text{ erg s}^{-1} \text{ Hz}^{-1}}. \quad (9)$$

To derive SFR_{2000} , we need the dust extinction at 2000 Å (Eq. 8). We use two approaches: the MW extinction law and the Calzetti law (Calzetti 2001) derived from a sample of local starbursts. The MW extinction is more appropriate for a uniform foreground screen of dusty gas (with covering factor 1). In this case, using $A_V = 0.6$ obtained from the Fe II column density, we derive $E_{B-V} = 0.19$. On the other hand, if the covering factor of the gas is < 1 , then the dust extinction is patchy and differs on average from the one derived from the dust depletion in the gas. In this case we use $E_{B-V} = 0.44$, the mean value derived from a sample of local starbursts (Calzetti et al. 1994). For both cases we obtain $A_{2000} \sim 1.7$ magnitudes. SFRs are given in Table 1; the mean (and median) value is $36 \text{ M}_\odot \text{ yr}^{-1}$. For the subsample of galaxies with measured [O II] emission, the mean is $32 \text{ M}_\odot \text{ yr}^{-1}$, close to the $40 \text{ M}_\odot \text{ yr}^{-1}$ derived from the [O II] emission. A $\sim 1.7\sigma$ significant linear correlation is found between the two sets of star formations (with $\text{SFR}_{[\text{OII}]} \sim 1.2 \text{ SFR}_{2000}$). Our SFR_{2000} is measured from the aperture corrected photometry, that includes the UV flux from a large part of the galaxy. The consistency with values derived from the [O II] observed in the spectra (these are associated with the smaller H II regions) suggests a high degree of mixing between the gas and the stars.

8.4. Spectral slope in GDDS galaxies

If the flux can be approximated by the power law $f_\lambda \propto \lambda^\beta$, we can estimate the spectral slope β in the individual spectra. The observed spectral range is not very large, 5000–9800 Å, therefore the spectral slope measured from there can be inaccurate, also because the flux calibration in MOS data is not perfect. However, we can use the observed Vega V and I magnitudes to derive β . If the AB magnitudes are $V_{AB} = V + 0.02$ and $I_{AB} = I + 0.45$, then β is:

$$\beta = 0.4 \times \frac{I - V + 0.43}{\log(\lambda_V / \lambda_I)} - 2 \quad (10)$$

where $\lambda_V = 5500$ Å and $\lambda_I = 8000$ Å. For a galaxy at $z = 1.6$, β would measure the spectral slope in the rest-frame interval 2100–3100 Å. For the individual 13 GDDS galaxies we obtain a mean value $\langle \beta \rangle = -1.15$ with a large dispersion of 0.9. In local star-forming galaxies, Calzetti et al. (1994) have measured β in a sample of 39 local starbursts in the wavelength range 1250–2600 Å. From this sample we derive a mean value $\langle \beta \rangle = -1.05$, with a dispersion of 0.65. At high redshift Shapley et al. (2003) derived β in LBGs using the intrinsic UV colors ($\lambda \sim 1200$ –1800 Å) and found $-1.1 < \beta < -0.7$. To compare our spectral slope to those found at lower wavelengths, we computed spectra using stellar synthesis models. We assumed a simple stellar population, with Salpeter IMF and continuous star formation. The spectral slope in the range $\lambda \sim 1200$ –2000 Å is slightly flatter than in the range $\lambda \sim 2000$ –3000 Å, due the contamination by strong stellar absorptions at $\lambda = 1200$ –2000 Å.

By applying the MW and starburst dust extinction laws, as described in the previous section, we calculated an intrinsic spectral slope in the interval $\lambda \sim 2100$ –3100 Å for our GDDS galaxies $\beta_i = -2.1$ and -2.0 , respectively.

Dunne, Eales, & Edmunds (2003) have found from submillimetre surveys that dust content was much higher in the past, therefore most of the metal rich systems cannot be found in surveys that are too shallow, or too sensitive to dust obscuration. GDDS cannot detect galaxies or regions of galaxies that are strongly obscured, so it is certainly affected by dust, but probably much less than other galaxies surveys, because it is unbiased and highly complete for galaxies with $K < 20.6$.

9. SUMMARY AND CONCLUSIONS

The GDDS (Abraham et al. in preparation) is a public survey that uses GMOS at Gemini, combined with the Nod & Shuffle technique, to study the properties of galaxies in the redshift desert ($0.8 < z < 2.0$). The GDDS observed galaxies with $I_{AB} \leq 24.8$ and $K < 20.6$, and is the most sensitive survey focused on the redshift desert obtained so far. The $K20$ survey obtained at the Very Large Telescope (VLT) is aiming at a similar scientific objective (Cimatti et al. 2002a) with 82 spectroscopically confirmed galaxies in the redshift desert in 52 arcmin². In the first two GDDS fields observed, 60.5 arcmin² and 59.5 hours exposure time, we identified 68 galaxies with spectroscopically-confirmed redshift. Among these, 34 are at $1.3 < z < 2.5$ (0.56 galaxies arcmin⁻²), whereas the $K20$ (17 VLT nights) identified 17 galaxies (0.32 galaxies arcmin⁻²) in the same redshift interval, showing the high efficiency of GDDS.

In this work, we have selected the UV brightest (AB absolute magnitude $M_{2000} < -19.65$) subsample with 13 galaxies that are in the redshift range $1.34 < z < 1.97$ ($\langle z \rangle = 1.60$) in order to study heavy elements in the neutral ISM. The selected galaxies are the most massive in the sample ($M \gtrsim 10^{10} M_{\odot}$) and represents between 25 and 38% of the total number of galaxies found in the $z > 1.3$ range (depending whether galaxies with tentative or photometric-only redshifts are included or not). Only three of these 13 galaxies have $K < 20.0$.

We detected strong [O II] emission associated with H II regions, with absolute luminosities ranging $5 - 40 \times 10^{41}$ erg s⁻¹, and roughly estimated $SFR = 13 - 106 M_{\odot} \text{ yr}^{-1}$ and $\langle SFR \rangle \sim 40 M_{\odot} \text{ yr}^{-1}$. The mean value is close to the mean value derived using UV luminosities found from the aperture-corrected photometry ($32 M_{\odot} \text{ yr}^{-1}$). This supports the assumption that on average the gas in the H II regions and the UV emitting stars are well mixed.

The stack of the 13 spectra shows Fe II, Mg II, Mn II, and Mg I absorption. The column density of Fe II and Mn II provide a good measure of the total column density of iron and manganese in the neutral ISM. We found $\log N_{\text{FeII}} = 15.54^{+0.23}_{-0.13}$ and $\log N_{\text{MnII}} = 13.49 \pm 0.13$. These values are larger than what typically measured in absorption systems along QSO sight lines (QSO-DLAs). Only 2 out of 24 at $1.0 < z < 2.0$ have similar Fe II column densities. On the other hand, high column densities are found in other star-forming objects. The Lyman break galaxy cB58 has $\log N_{\text{FeII}} = 15.25$, while GRB host galaxies (GRB-DLAs) have $\log N_{\text{FeII}} = 14.8 - 15.9$. From the depth of the Mg II absorption, we derived a conservative lower limit to the ISM filling factor of 70%.

The high filling factor of the ISM and the consistency between SFRs derived from [O II] and UV emission, suggests a homogeneous distribution of stars and gas. If we assume that the mean H I column density in the ISM is $\log N_{\text{HI}} < 21.7$ (as in 98% of QSO-DLAs), the mean metallicity would be $Z/Z_{\odot} > 0.2$ for a moderate Fe dust depletion correction ($\delta_{\text{Fe}} = 1$ dex). High metallicities ($Z/Z_{\odot} = 0.5 - 2$) are also

found in H II regions of galaxies at $0.3 < z < 0.9$ (Kobulnicky et al. 2003; Lilly et al. 2003).

From the Fe II column density, we estimated an optical dust obscuration $A_V \sim 0.6$ mag. The mean spectral slope in our GDDS galaxies around the 2100–3100 Å interval is $\beta \sim -1.15$, from which we derive an intrinsic dust corrected mean spectral slope $\beta \sim -2$.

When completed, the GDDS will provide observations of two additional fields. From the full data set we will detect or give significant limits on other absorption lines. For instance, the Zn II detection at ~ 2000 Å, or Si II at $\lambda \sim 1800$ Å, are powerful diagnostics for metal enrichment and dust depletion. GDDS galaxies and GRB-DLAs are clearly probing high- z galaxies with a strong star formation activity, for which metal enrichment and/or dust obscuration can be higher than in the QSO-DLA population. Our conclusion is that direct detections of galaxies, and indirect through QSO absorption lines, provide a more complete picture of the galaxy census in the high redshift Universe. The former can be seen only if star formation is high, the latter only when metal enrichment is low.

This paper is based on observations obtained at the Gemini Observatory, which is operated by the Association of Universities for Research in Astronomy, Inc., under a cooperative agreement with the NSF on behalf of the Gemini partnership: the National Science Foundation (United States), the Particle Physics and Astronomy Research Council (United Kingdom), the National Research Council (Canada), CONICYT (Chile), the Australian Research Council (Australia), CNPq (Brazil), and CONICET (Argentina).

We are grateful to the entire staff of the Gemini Observatory for the kind hospitality and support during our visits. We thank Matt Mountain, Jean-René Roy, and Doug Simons for support of the program (including the Director's Discretionary Time allocated to GDDS), Matthieu Bec and Tatiana Paz for technical modifications to the GMOS telescope control system, and Richard Wolff for work on the detector controller. We acknowledge the anonymous referee for thoughtful comments that greatly improved the discussion. We thank A. Aloisi, C. Hoopes, N. Masetti, and N. Walborn for interesting insights. S.S. acknowledges generous funding from the David and Lucille Packard Foundation. H.-W.C. acknowledges support by NASA through a Hubble Fellowship grant HF-01147.01A from the Space Telescope Science Institute, which is operated by the Association of Universities for Research in Astronomy, Incorporated, under NASA contract NAS5-26555.

REFERENCES

- Aloisi, A., Savaglio, S., Heckman, T. M., Hoopes, C. G., Leitherer, C., & Sembach, K. R. 2003, *ApJ*, 595, 760
- Barth, A. J., et al. 2003, *ApJ*, 584, L47
- Blades, J. C., Hunstead, R. W., Murdoch, H. S., & Pettini M. 1982, *MNRAS*, 200, 1091
- Bloom, J. S., Kulkarni, S. R., & Djorgovski, S. G. 2002, *AJ*, 123, 1111
- Bohlin, R. C., Savage, B. D., & Drake, J. F. 1978, *ApJ*, 224, 132
- Calzetti, D. 2001, *PASP*, 113, 1449
- Calzetti, D., Kinney, A. L., & Storchi-Bergmann, T. 1994, *ApJ*, 429, 582
- Castro, S., Galama, T. J., Harrison, F. A., Holtzman, J. A., Bloom, J. S., Djorgovski, S. G., & Kulkarni, S. R. 2003, *ApJ*, 586, 128
- Daddi, E., et al. 2003, *ApJ*, in press (astro-ph/0308456)
- Chen, H.-W., et al. 2002, 570, 54
- Chen, H.-W., et al. 2003, *ApJ*, 586, 745
- Churchill, C. W., Vogt, S. S., & Charlton, J. C. 2003, *AJ*, 125, 98
- Cimatti, A., et al. 2002a, *A&A*, 381, L68
- Cimatti, A., et al. 2002b, *A&A*, 392, 395
- Cuillandre, J. C., et al. 1994, *A&A*, 281, 603
- de Mello, D. F., Leitherer, C., Heckman, T. M. 2000, *ApJ*, 530, 251
- Dickinson, M., Papovich, C., Ferguson, H. C., & Budavari, T., 2003, *ApJ*, 587, 25
- Ding, J., Charlton, J. C., Bond, N. A., Zonak, S. G., & Churchill, C. W. 2003, *ApJ*, 587, 551
- Djorgovski, S. G., et al. 2003, Proceedings of workshop "Gamma-Ray Bursts in the Afterglow Era: 3rd Workshop", ASPCS, in press (astro-ph/0302004)
- Dunne L., Eales, S. A., & Edmunds, M. G., 2003, *MNRAS*, 341, 589
- Eisenstein, D. J., et al. 2003, *ApJ*, 585, 694
- Ellison, S. L., Yan, L., Hook, I. M., Pettini, M., Wall, J. V., & Shaver, P. 2001, *A&A*, 379, 393
- Faber, S. M., Friel, E. D., Burstein, D., & Gaskell, C. M. 1985, *ApJSS*, 57, 711
- Firth, A., et al. 2002, *MNRAS*, 332, 617
- Fontana A., et al. 2003, *ApJL*, 594, L9
- Fukugita, M., Hogan, C. J., & Peebles, P. J. E. 1998, *ApJ*, 503, 518
- Fynbo, J., et al. 2002, in Lighthouses of the Universe: Proc. MPA/ESO/MPE/USM Joint Astronomy Conf., ed. M. Gilfanov, R. A. Siunjaev, & E. Churazov (Berlin: Springer), 187
- Gallagher, J. S., Hunter, D. A., & Bushouse, H. 1989, *AJ*, 97, 700
- Gallego, J., Zamorano, J., Aragón-Salamanca, A., & Regg, M. 1995, *ApJ*, 455, L1
- Giallongo, E., Cristiani, S., D'Odorico, S., & Fontana, A. 2002, *ApJ*, 568, L9
- Glazebrook, K., Blake, C., Economou, F., Lilly, S., & Colless, M. 1999, *MNRAS*, 306, 843
- Glazebrook, K. & Bland-Hawthorn, J. 2001, *PASP*, 113, 197
- Grevesse, N., & Sauval, A. J. 1998, *Space Sci. Rev.*, 85, 161
- Heckman, T. M., Robert, C., Leitherer, C., Garnett, D. R., & van der Rydt, F. 1998, *ApJ*, 503, 646
- Heckman, T. M., Sembach, K. R., Meurer, G. R., Strickland, D. K., Martin, C. L., Calzetti, D., & Leitherer, C. 2001, *ApJ*, 554, 102
- Hicks, E. K. S., Malkan, M. A., Teplitz, H. I., McCarthy, P. J., & Yan, L. 2002, *ApJ*, 581, 205
- Hjorth, J., et al. 2003, *ApJ*, in press (astro-ph/0307331)
- Hook, I. M., et al. 2003, *SPIE*, 4841, 1645
- Jansen, R. A., Franx, M., & Fabricant, D. 2001, *ApJ*, 551, 825
- Jenkins, E. B. 1986, *ApJ*, 304, 739
- Jensen, B. L., et al. 2001, *A&A*, 370, 909
- Jha, S., et al. 2001, *ApJ*, 554, L155
- Kennicutt, R. C. 1992, *ApJ*, 388, 310
- Kennicutt, R. C. 1998, *ApJ*, 498, 541
- Kobulnicky, H. A., & Koo, D. C. 2000, *ApJ*, 545, 712
- Kobulnicky, H. A., et al. 2003, *ApJ*, in press (astro-ph/0305024)
- Kulkarni, S. R., et al. 1999, *Nature*, 398, 389
- Lilly, S. J., Carollo, C. M., & Stockton, A. N. 2003, *ApJ*, in press (astro-ph/0307300)
- Lu, L., Sargent, W. L. W., Barlow, T. A., Chruchill, C. W., & Vogt, S. S. 1996, *ApJS*, 107, 475
- Malkan, M., Webb, W., & Konopacky, Q. 2003, *ApJ*, in press, (astro-ph/0310237)
- Masetti, N., et al. 2001, *A&A*, 374, 382
- McCarthy, P., et al. 2001, *ApJ*, 560, L131
- McWilliam, A., Rich, R. M., & Smecker-Hane, T. A. 2003, *ApJ*, 592, L21
- Mirabal, N., et al. 2002, *ApJ*, 578, 818
- Peroux, C., McMahon, R. G., Storrie-Lombardi, L. J., & Irwin, M. J., 2003, *MNRAS*, in press, (astro-ph/0107045)
- Pettini, M., Kellogg, M., Steidel, C. C., Dickinson, M., Adelberger, K. L., & Giavalisco, M. 1998, *ApJ*, 508, 539
- Pettini, M., Rix, S. A., Steidel, C. C., Adelberger, K. L., Hunt, M. P., & Shapley, A. E. 2002, *ApJ*, 569, 742
- Pettini, M., Smith, L. J., King, D. L., & Hunstead, R. W. 1997, *ApJ*, 486, 665
- Pozzetti L., et al., 2003, *A&A*, 402, 837
- Prochaska, J. X., et al. 2001, *ApJS*, 2001, 137, 21
- Prochaska, J. X., Gawiser, E., Wolfe, A. M., Castro, s., & Djorgovski, S. G. 2003b, *ApJ*, 595, L9
- Prochaska, J. X., Gawiser, E., Wolfe, A. M., Cooke, J., & Gelino, D. 2003a, *ApJS*, 147, 227
- Prochaska, J. X., & Wolfe, A.M. 1999, *ApJS*, 121, 369
- Rao, S. M., & Turnshek, D. A. 2000, *ApJS*, 130, 1
- Salamanca, I., et al. 2001, *MNRAS*, submitted
- Savage, B. D., & Sembach, K. R. 1991, *ApJ*, 379, 245
- Savage, B. D., & Sembach, K. R. 1996, *ARA&A*, 34, 279
- Savaglio, S., Fall, S. M., & Fiore F. 2003, *ApJ*, 585, 638
- Savaglio, S., Panagia, N., & Padovani, P. 2002, *ApJ*, 567, 702
- Sembach, K. R., & Savage, B. D. 1996, *ApJ*, 457, 211
- Shapley, A. E., Steidel, C. C., Pettini, M., & Adelberger, K. L. 2003, *ApJ*, 588, 65
- Spitzer, L. 1978, *Physical Processes in the Interstellar Medium* (New York: Wiley)
- Spitzer, L., & Fitzpatrick, E. L. 1995, *ApJ*, 445, 196
- Steidel, C. C. 1990, *ApJS*, 72, 1
- Steidel, C. C., Adelberger, K. L., Shapley, A. E., Pettini, M., Dickinson, M. E., & Giavalisco, M. 2003, *ApJ*, 592, 728
- Steidel, C. C., & Sargent, W. L. W. 1992, *ApJS*, 80, 1
- Storrie-Lombardi, L. J., & Wolfe, A. M. 2000, *ApJ*, 543, 552
- Tremonti, C. A., Leitherer, C., Heckman, T. M., & Calzetti, D. 2003, *ApJ*, submitted
- Turnshek, D. A., Wolfe A. M., Lanzetta K. M., Briggs, F. H., Cohen, R. D., Foltz, C. B., Smith, H. E., & Wilkes, B. J. 1989, *ApJ*, 344, 567
- Vazdekis, A. 1999, *ApJ*, 513, 224
- Vreeswijk, P. M., et al. 2001, *ApJ*, 546, 672
- Vreeswijk, P. M., et al. 2003, *A&A*, submitted
- Welty, D. E., Frisch, P. C., Sonneborn, G., & York, D. G. 1999, *ApJ*, 512, 636
- Welty, D. E., Lauroesch, J. T., Blades, J. C., Hobbs, L. M., & York, D. G. 1997, *ApJ*, 489, 672
- Zwaan, M. A., et al. 2003, *AJ*, 125, 2842